

École d'ingénieur Polytech Nice Sophia

---

Ingénieur en 5<sup>ème</sup> année en Génie de l'Eau - Parcours Hydroinformatique

**Impact of coupling an actual evapotranspiration model with a lumped hydrological model to improve hydrological simulations**

**Peng HUANG**

**Encadrantes: Maria-Helena RAMOS**

**Daniela PEREDO**

**Encadrant académique: Pierre BRIGODE**

**Septembre 2018**



<b>IRSTEA</b>	<b>Polytech Nice Sophia</b>
<b>U. R. HYCAR</b>	<b>Département Génie de l'eau</b>
1 Rue Pierre Gilles de Gennes	930 Route des Colles
92761 Antony - France	06410 Biot - France

## About IRSTEA

IRSTEA (*Institut National de Recherche en Sciences et Technologies pour l'Environnement et l'Agriculture*), National Research Institute of Science and Technology for Environment and Agriculture, conducts research to answer agro-environmental questions posed in the fields of water, natural risks, regional planning and environmental technologies.

Multidisciplinary, action-oriented and in support of public policies, its research and expertise activities involve a strong partnership with French and European universities and research organizations, economic sections and public authorities. The institute is a founding member of the AllEnvi National Research Alliance for the Environment and member of the European PEER Network. It has been labeled "Institut Carnot" since 2006. A public scientific and technological institution, *IRSTEA* is placed under the dual supervision of the ministries in charge of research and agriculture.

The work described in this internship's report was carried out at IRSTEA's research center in Antony, within the Catchment Hydrology research team (<https://webgr.irstea.fr>) and the HYCAR research unit, both under the umbrella of the Water Department.

## **Abstract**

Evapotranspiration is a major component in both the water balance and the energy balance of the hydrological system. How to improve hydrological simulations and projections from a better estimation of evapotranspiration remains a crucial challenge. This study explores the impact of using actual evapotranspiration forcing in a hydrological model, compared with using potential evapotranspiration data. The estimation of actual evapotranspiration is based on an energy-balance model (the MEP model) and the hydrological simulations are based on a water-balance hydrological model. We investigate how coupling both models impact low and high flow simulations. Various statistical metrics are employed to quantify and analyze the results: the Nash-Sutcliffe efficiency, the Kling-Gupta efficiency, the percent bias, the rooted mean square error and the coefficient of determination. Findings from this study suggest that the use of actual evapotranspiration can provide better results in hydrological simulation. The coupled model shows a good performance in modeling soil moisture and actual evapotranspiration, while the hydrological simulations (low and high flows) are less impacted by the use of the coupled model. Further analyses are needed in order to reduce the inherent errors in the atmosphere-land coupling mechanism and improve hydrological simulations.

**Keywords:** Evapotranspiration, water balance, energy balance, hydrological modeling

## **Acknowledgements**

I would first like to express my sincere gratitude to my internship supervisors Maria-Helena RAMOS research scientist, and her PhD student Daniela PEREDO for their immense knowledge, useful remarks and engagement through the whole process of my internship. These words are not enough to describe the help they gave me and it is a great honor to work with them.

I would also like to thank Pierre BRIGODE, Associate Professor at Université de Nice Sophia Antipolis, as the second reader of this report. I am grateful for his very valuable comments.

Besides, my sincere thanks go to Alain GUERIN, a retired colleague who helped me with data processing and analysis before retiring from IRSTEA, and Olivier DELAIGUE, teammate of the HYCAR research unit, who helped with the acquisition of the data needed in my study.

Thanks also to all my colleagues in IRSTEA. You were very helpful and friendly. I miss the moments when we played volleyball, frisbee and ping-pong during the lunch break. The comfortable working ambiance and the joyous experiences shall be an unforgettable memory in my student career.

In the end, I acknowledge Météo-France for the SAFRAN data archive, IRSTEA for the BDOH\_ORACLE hydrological data and MODIS for the NDVI data.

# Summary

<b>1. Introduction</b>	<b>1</b>
<b>2. Literature Review</b>	<b>2</b>
2.1. Evapotranspiration in hydrological modeling	2
2.2. From potential evapotranspiration to actual evapotranspiration	3
2.3. Evapotranspiration under global warming	4
2.4. Summary of the literature	4
<b>3. Methodology</b>	<b>5</b>
3.1. General introduction	5
3.2. The MEP (Maximum Entropy Production) model	6
3.3. GR hydrological models	7
3.3.1. Interception reservoir	7
3.3.2. GRHUM model production reservoir	7
3.3.3. GR4H model	10
3.4. Model coupling	11
3.5. Model assessment	12
<b>4. Materials</b>	<b>13</b>
4.1. Study Area: Les Avenelles catchment	13
4.2. MEP input data and AET field observations	15
4.3. Data for the calibration of the GR4H model	16
4.4. Normalized Difference Vegetation Index (NDVI)	17
4.5. Data Summary	18
<b>5. Results</b>	<b>19</b>
5.1. Input data analysis	19
5.2. Validation of the MEP model	20
5.3. MEP-GR4H modeling chain	23
5.4. The coupled model (MEP-I-GRHUM-GR4H)	26
<b>6. Discussion and Conclusion</b>	<b>34</b>
<b>7. Reference</b>	<b>36</b>
<b>8. Appendix</b>	<b>41</b>

## 1. Introduction

Evapotranspiration (ET), a process that involves physical evaporation and vegetal transpiration, is a major component in the water circulation and energy balance. At the continental scale, approximately 2/3 of annual precipitation is evaporated into the atmosphere, along with the consumption of half of the available net radiation (Seguin, 1997). Accurate ET estimation is therefore fundamental not only for water resources evaluation and management, but also as it plays an important role in drought monitoring and hydrological projection (Maidment, 1993).

ET processes play an important role in both water-balance and energy-balance systems. Both provide the basic principles of ET estimation. Water-balance models (e.g., hydrological models) focus on mass conservation to quantitatively estimate ET while energy-balance methods focus on the analysis of the energy budget of the Earth. Most tools using methods of ET estimation are based on a single principle. Either they are based on water-balance method or on energy-balance method. Therefore, the integration of an energy-balance model to a hydrological model to have both the energy conservation and the mass conservation principles considered altogether is a key point for research and applications in water modeling.

How to improve the hydrological performance of a model by using a more accurate ET estimation remains a crucial challenge in hydrology. As actual evapotranspiration (AET) is difficult to measure, an indirect way to estimate it is usually adopted from the potential evapotranspiration (PET), which determines the upper limit of AET, often employed as input data in hydrological modeling. However, this approach seems to be less capable nowadays to capture the impacts of climate changes on simulated river flows due to the sensitivity of hydrological projections to different PET inputs. Many studies reveal the importance of testing the applicability of various PET formulas in hydrological modelling under climate change (e.g., Guo *et al.*, 2017; Seiller and Actil, 2016; Bai *et al.*, 2016; Bartholomeus *et al.*, 2015). It seems therefore complex to determine an ultimate or a universal PET formula that could suit all situations encountered in hydrological modeling, as large dissimilarities can be observed among catchments and different climatic conditions.

A new perspective towards changing the use of PET in hydrological models was investigated by Peredo (2017), whose work addressed the question: what is the impact of the straightforward use of AET input on a lumped hydrological model? The feasibility of a direct AET input was investigated by chaining an energy balance model (MEP model) to a lumped hydrological model (GR4H model) on an experimental catchment monitored by IRSTEA. Results from this work showed that low flow simulations can be improved by using an AET model. The work was however based on a short (less than one year) time series of data and without a formal model coupling approach. Further analyses were therefore recommended.

Our study is based on what was done in the work of Peredo (2017) and on the perspectives that emerged from it. The estimation of AET is also based on the MEP model, an energy-balance model, firstly suggested by Wang and Bras (2011) and improved by Hajji *et al.* (2017), which considers both evaporation and transpiration

processes. Further, this study aims at investigating how this energy-balance semi-physical model can provide a useful estimation of AET to a water-balance conceptual hydrological model. In other words, we investigate how this MEP model efficiently interacts with the hydrological model and impacts hydrological simulations. To achieve this objective, the hydrological model should be capable of integrating the information provided by the energy-balance model. The interaction processes between the two model domains can be represented with the help of “model coupling”. Different parts of the conceptual hydrological models of the GR family of models developed at IRSTEA (see, for instance, Coron *et al.*, 2017) are incorporated into the coupling framework. Thus, our study focuses on coupling the different models, as well as using several heuristic parameterizations to simplify the operation, and better represent the water flux in atmosphere-vegetation-soil interactions.

This study is divided into two parts: firstly, we simulate the AET for the years 2016-2017 and validate the MEP model to extend the study period of the work by Peredo (2017); secondly, we couple the MEP model with the water-balance hydrological model and evaluate its impact on the simulations of the coupled model. Section 2 presents the basic theories of ET in hydrological modeling, uncertainties of PET as an input data in hydrological modeling and the importance of ET to hydrological simulations and climate change studies. Section 3 discusses the principles of model coupling, and presents detailed descriptions of the MEP model as well as of the hydrological models uses. We also describe how the MEP model is coupled with hydrological models in our study. Section 4 presents the study area and the data used in this study. The results and the conclusions of this study are presented in Section 5 and Section 6, respectively.

## **2. Literature Review**

### **2.1. Evapotranspiration in hydrological modeling**

Theoretically, AET is a major subtractive element to a regional system in the water-balance framework. It is difficult to measure and currently only methods such as the Eddy Covariance and the Energy Balance Bowen Ratio, devices such as weighable lysimeters and scintillometers, or functions based on Surface Water Balance and Atmosphere Water Balance can provide continuous estimation of AET (Wang and Dickson, 2012). Given current constrains, such as high installation or maintenance cost, high data-requirement and various uncertainties, the estimation of AET in rainfall-runoff models is often performed from applying the soil moisture extraction function in PET formula as an indirect way to obtain AET. On the other hand, PET (e.g., Penman-Monteith formula; Monteith, 1965) estimates the atmospheric demand for water from a saturated surface, mainly considering the meteorological parameters such as temperature, wind speed, specific humidity and solar radiation. Therefore, the application of PET is pragmatic and operationally simple, thanks to the availability of these meteorological parameters to estimate its value (Oudin, 2004).

Up to now there are two main ways to estimate AET at a catchment scale in hydrological models. The first one calculates, separately, water surface evaporation, soil evaporation and vegetation transpiration and then integrates them together to estimate the basin ET. This approach is usually applied in physically-based

hydrological models. The second approach to estimate AET is based on the PET formula and soil moisture functions. It is usually applied in conceptual models (Zhao *et al.*, 2013). Improvements have been made on AET estimations in hydrological models by including remotely-sensed data to distributed (e.g., Chen *et al.*, 2005) and lumped rainfall-runoff models (e.g., Zhang *et al.*, 2009). This improvement with remote sensing data is however limited by the time scale requirements of the models and the lack of instantaneousness remote-sensed data and the low accuracy problem of available data.

## **2.2. From potential evapotranspiration to actual evapotranspiration**

As an important forcing data in hydrological simulation, PET has drawn a lot of attention (e.g., Singh and Xu, 1997; Andréassian *et al.*, 2004). Nonetheless, concerning the use of PET in hydrological simulation, three main obstacles exist:

- Firstly, insensitivity of rainfall-runoff models to PET input has been verified and intensively investigated (e.g., Fowler, 2002). The reasons why most rainfall-runoff models do not provide a better simulation with a more detailed PET input may be related to: (1) a natural phenomenon convey, (2) an inherent defect of models or/and (3) an inappropriate PET estimation (Oudin *et al.*, 2005a). The first explanation is more commonly accepted, which reveals that soil moisture is a core factor in ET processes. Parmele (1972) and Paturel *et al.* (1995) attributed this insensitivity dilemma to the soil moisture pattern in models that work as a low-pass filter. Oudin *et al.* (2004; 2005b) challenged the efficiency and validity of the Penman-Monteith formula, even though it is a physically-based formula. In addition, soil moisture pattern still shows a considerable efficiency during the conversion from PET to AET in rainfall-runoff models (Oudin *et al.*, 2005). Given this insensitivity, simpler and less physically based PET methods are prone to be applied in discharge simulation (Kannan *et al.*, 2007; Kay and Davies, 2008). Although the simplification of the estimation of PET is attractive, no solid evidence confirms the accuracy and validity of this input. The comparison of model performance to an AET input has not yet been conducted and whether this input is capable of projecting future climate impact is still an open question (Seiller and Anctil, 2016).

- Secondly, the use of PET as an input to hydrological models adds uncertainties to some extent and this remains a crucial problem when dealing with future climate projections (Kingston *et al.*, 2009). The double source of uncertainties, due to the choice of PET formula and the transformation to AET from the soil water content, makes it difficult to accurately represent the land-atmosphere interaction. The poor simulation of prolonged low flow and recession periods in rainfall-runoff models may probably be ascribed to this, as the ET process dominates in drought periods. Numerous PET formulas exist based on different driven mechanisms. Zhao *et al.* (2013) summarized the formulas used in hydrological models and showed that the selection of a competent PET formula, as well as a soil moisture function, to reduce uncertainties remains a pivotal question.

- Thirdly, the term PET itself is quite ambiguous, without a full consideration of the vegetal transpiration (Brutsaert, 1982). The concept of PET was firstly introduced by

Thornwaite (1948) for the classification of climate and it is now widely used as a maximum rate of AET. A considerable difference between evaporation and ET has been found over tall vegetation (e.g., Stewart and Thom, 1973), as well as for the ET in forested and grassed areas (Zhang *et al.*, 2001). The simplification brought by ignoring the effect of transpiration seems unacceptable, especially in vegetation-covered catchments. Recent work (Jasechko *et al.*, 2013) has showed that transpiration itself accounts for up to 90% of terrestrial ET and water losses through transpiration into the atmosphere should be fully taken into consideration in hydrological simulation. Even though several PET formulas with consideration of transpiration were proposed, such as Turc (1961) and Hamon (1961), they are just suitable for specific underlying surface and climate conditions.

The three main obstacles mentioned above hamper the improvement of modeling in energy- and water-balance frameworks. Whether PET as forcing data is appropriate and robust enough to simulate the hydrological processes within a catchment or to project the impact of climate change still requires deep investigations.

### **2.3. Evapotranspiration under global warming**

Nowadays, the trend of global warming is inevitable and its impact on the ET process of the terrestrial hydrological cycle is remarkable (IPCC, 2014). The potential alterations in regional ET have been studied in abundance (e.g., Sharma and Walter, 2014). It is broadly acknowledged that current warming climate is accelerating the hydrological cycle and the AET tends to increase during the past several decades in most places, associated with the observed increase in precipitation (e.g., Golubov *et al.*, 2001; Koster *et al.*, 2004; Qian *et al.*, 2007; Van Heerwaarden *et al.*, 2010).

However, some opposite trends in PET and AET are reported (Liu *et al.*, 2004; Roderick and Farquhar, 2002; Xu *et al.*, 2005; Van Heerwaarden *et al.*, 2010). A decreasing trend in pan evaporation has been reported worldwide (known as the evaporation pan paradox), which indicates the reduced evaporative demand or PET (Liu *et al.*, 2004). Contradictory to the global warming, a decreasing solar radiation (global dimming) may be linked to the pan evaporation anomalies (e.g., Roderick and Farquhar, 2002; Xu *et al.*, 2005; Van Heerwaarden *et al.*, 2010). Hobbins *et al.* (2004) suggested that this inconsistency is just a complementary demonstration of increased AET, which defend the standpoint of Brutsaert and Parlange (1998): decreasing pan evaporation actually indicates increasing terrestrial evaporation.

In short, estimating AET from the evaporative demand is inadequate nowadays as the ET process is dominated not only by the energy budget but also by water supply limitations (Roderick *et al.*, 2009a; 2009b).

### **2.4. Summary of the literature**

In summary, the literature identifies the uncertainties of using PET in hydrological simulations and future projections as well as the importance of accurate ET estimation in the current climate and a changing climate context. The use of PET in hydrological modeling as an indirect way to solve the problem of the difficult availability of continuous AET data has showed a great success. However, the use of PET in

hydrological modeling seems less and less capable of meeting the needs of projection accuracy and providing the full information of hydrological components. Therefore, moving from PET to AET as forcing data to hydrological models to simulate the present and to project the future tends to be more reasonable due to the fact that AET greatly reduces the input uncertainty in the modeling framework.

### **3. Methodology**

#### **3.1. General introduction**

In hydro-meteorological research and forecasting activities, which consider local atmosphere-land interactions, advanced models are needed. Conjunctive modeling is a major methodology in “modeling and simulation” used to integrate systems or processes. Conjunctive modeling means to “link site-specific models in such a way that the interaction processes, between the domains the models represent are modeled on a time-step basis” (Becker and Burzel, 2016).

There are two main types of conjunctive modeling: one is model coupling, which means that models are fully coupled with bi-directional data transmission; the other one is one-way chain, an uncoupled approach that has data exchange in one direction only (Becker and Burzel, 2016). For instance, if we consider two models that need to be conjunctively linked, if models are coupled, the simulation results of the first model have an impact on the second model and vice versa. This means that coupled models must exchange information during runtime on a time step basis. If models are uncoupled, the simulation results of the first model have an impact on the second one, but the simulation results of the second model have no feedback impact on the first model (Becker and Burzel, 2016).

The coupling of models is a commonly used approach when addressing the complex interactions between different components of earth systems (e.g., Zabel and Mauser, 2012). The work by Givati *et al.* (2016) has suggested that the use of model coupling in atmospheric-hydrological simulations has the potential to improve forecasts for early flood warning, compared with the use of uncoupled models. It should be noted that coupled models are considerably harder to develop than the one-way chain as there is much more possibility for the coupled model to alienate away from the reality.

As mentioned in section 2, since soil moisture content has profound effects on ET process, and since ET process creates significant subtraction (addition during the condensation) to the soil moisture, we propose to investigate how the soil moisture part of a hydrological model and the AET model should be coupled together to better simulate the atmosphere-land interactions and to gain an improved understanding of the model’s response dynamics. The MEP model, used to estimate AET, is divided into soil evaporation and vegetal transpiration, which subtract water content from surface soil and root-zone soil, respectively. As such, a two-layer system in the hydrological production reservoir, which can represent the evolution of soil moisture in these two layers, should be applied. For this, GRHUM model (Loumagne *et al.*, 1996) is chosen in our study. To better represent the atmosphere-vegetation-soil continuum, the coupled model obtained with the MEP and the GRHUM models will be embedded in the GR4H model structure (Perrin *et al.*, 2003). To make use of recent

research, we will also investigate the use of an interception reservoir introduced by Ficchi (2017). These models are described in the next sections and then the model coupling technique is explained.

### 3.2. The MEP (Maximum Entropy Production) model

Whereas the first law of thermodynamics expresses the conservation of energy, the second law specifically states that all isolated systems irreversibly act to dissipate. The dissipated potential is referred to as entropy. As any thermodynamic non-equilibrium system shall unceasingly develop to a steady state (thermodynamic equilibrium) over sufficiently long time, the notion of entropy is then the distance to the thermodynamic equilibrium. Entropy production can thus be interpreted as the degree of irreversibility. The proposed principle of the Maximum Entropy Production (MEP) model states that given the present constraints, a non-equilibrium system develops so as to produce entropy at the maximum possible rate. The second law of thermodynamics explicitly states the increasing trend of entropy while the MEP principle, as a complement to the second law of thermodynamics, answers which path, out of available paths, it will take (Swenson, 2000).

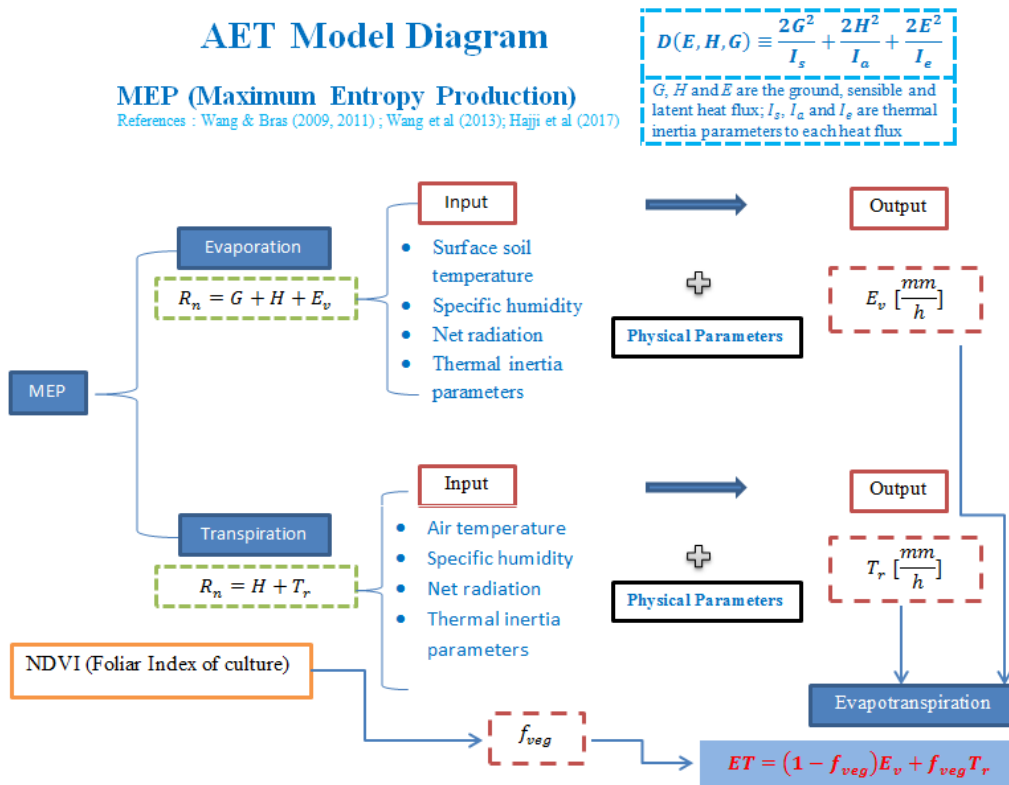


**Figure 1:** The diagram of the MEP model showing that the AET process restricted by energy balance function is estimated from soil evaporation and vegetal transpiration with an introduction of a vegetation index (modified from Peredo, 2017).

A state far from equilibrium is maintained in extremely complicated interactions in Earth systems (AET process, for example), where there remains a lack of full understanding of physical mechanisms behind these processes (Kleidon, 2009). Instead of figuring out the governing physical laws to describe events in sufficiently rigorous terms, a prediction of the evolution or a quantitative inference with the current limited information can be more promising.

Based on this, figure 1 shows how the MEP model is constructed as explained by Wang and Bras (2011), including evaporation from soil and transpiration from vegetation. A detailed model formulation is presented in *Appendix*.

### 3.3. GR hydrological models

Irstea<sup>1</sup>, has developed a set of lumped hydrological models, the “Génie Rural” (GR) family of models<sup>2</sup>. The GR models have shown a good performance in French basins and their simple structure allows the compatibility with other models. An interception reservoir introduced by Ficchi (2017), a two-layer production reservoir of the GRHUM model (Loumagne *et al.*, 1996) and the GR4H model (Perrin *et al.*, 2003) are presented below. As explained in the introduction section, since the MEP model should interact efficiently with the existing hydrological models, we decided to choose these models to carry out the tests of our work.

#### 3.3.1. Interception reservoir

Interception refers to precipitation that does not reach the soil, but is instead intercepted by the vegetation canopy. The interception reservoir introduced by Ficchi (2017) has a capacity of a few millimeters ( $I_{max}$ ) that needs to be calibrated. The reservoir produces net precipitation ( $P_n$ , in mm) when this capacity is exceeded. In our study, the interception loss ( $E_i$ , in mm), i.e. evaporation from the reservoir, is determined by the AET from the MEP model. The diagram of the interception reservoir is shown in figure 2.

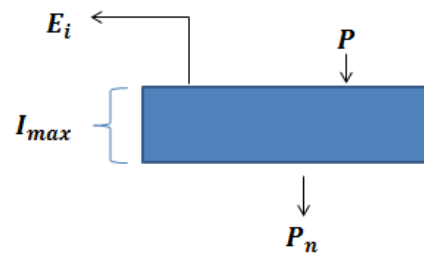


**Figure 2:** The diagram of the interception reservoir introduced by Ficchi (2017).

The implementation of the interception reservoir in our study depends on the priority given to interception loss. Thus, equations over a time step are:

The interception loss [mm] over a time step:

$$E_i = \min\left(AET, P + \frac{I_0}{\Delta t}\right) \quad (1)$$

The net precipitation rate [mm] over a time step:

$$P_n = \max\left(0, P - \frac{(I_{max} - I_0)}{\Delta t} - E_i\right) \quad (2)$$

The reservoir water content [mm] over a time step:

$$I = I_0 + (P - P_n - E_i)\Delta t \quad (3)$$

#### 3.3.2. GRHUM model production reservoir

The soil production reservoir is represented by a two-layer system for simulating

<sup>1</sup> National applied research institute in France.

<sup>2</sup> <https://hepex.irstea.fr/the-family-of-the-gr-hydrological-models/>

surface soil moisture  $W_s$  and global soil (bulk soil) moisture  $W_g$ . The production reservoir has a capacity of  $W_{smax}$  for surface soil moisture and a capacity of  $W_{gmax}$  for global soil moisture, which needs to be calibrated. The bulk layer represents the root zone where vegetal transpiration takes place and includes the topsoil. The depth of surface soil,  $d_s$ , and that of bulk soil,  $d_g$ , are fixed to 10 centimeters and 100 centimeters according to the local soil property (Loumagne *et al.*, 1996).

The entering source to the production reservoir is the net precipitation from the interception reservoir and thus the two reservoirs can be connected. Net precipitation is divided in two parts: the first one,  $P_s$ , wets the production reservoir via the transfer function; the other,  $P_n - P_s$ , goes directly to the outlet. The distribution of throughfall<sup>3</sup> is driven by the moisture state of the global layer.  $E_s$ , ET from the surface layer, and  $E_g$ , ET from the global layer, are calculated from the MEP model, based on the corresponding soil moisture. Percolation leakage from the topsoil,  $PR_s$ , and the one from the bulk soil,  $PR_g$ , are determined by the Thomas model (Thomas, 1981). Figure 3 shows the diagram of the production reservoir in the GRHUM model, as described in the works of Loumagne *et al.* (1996).

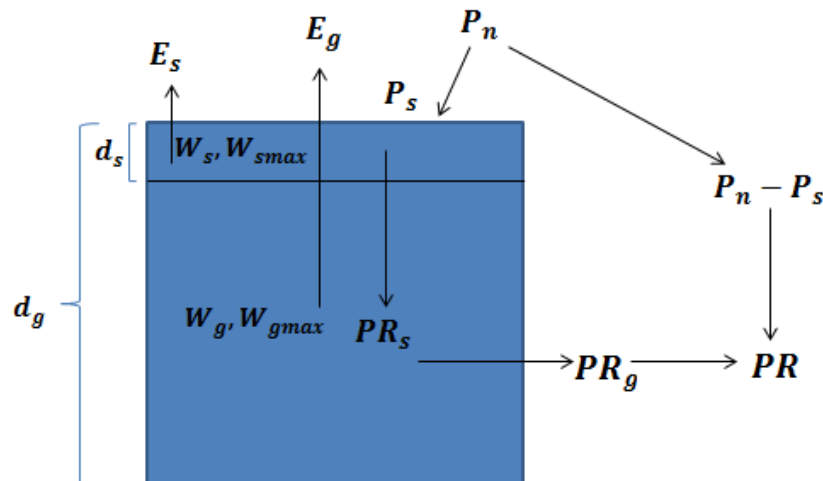


**Figure 3:** The diagram of the production reservoir in the GRHUM model (source: Loumagne *et al.*, 1996).

### 1) Soil moisture evolution

Throughfall feeds the production reservoir:

$$P_s = P_n - \left( \frac{W_g}{W_{gmax}} \right)^2 P_n \quad (4)$$

and therefore variations of surface and bulk layer humidity are obtained:

$$\begin{cases} \frac{\Delta W_s}{\Delta t} = \frac{P_s - E_s - PR_s}{d_s} \\ \frac{\Delta W_g}{\Delta t} = \frac{P_s - E_g - PR_g}{d_g} \end{cases} \quad (5)$$

<sup>3</sup> In hydrology, throughfall is the process which describes how wet leaves shed excess water onto the ground surface

The percolation produced by the topsoil infiltrates towards the bulk soil and the percolation produced by the bulk soil adds to the direct flow that goes to the outlet.  $PR_s$  and  $PR_g$  are defined in the Thomas model (Thomas, 1981), which is presented in the following.

## 2) Drainage function: Thomas model

In the case when throughfall is greater than global ET, humidity values from the soil layers are considered to temporarily increase to the value:

$$\begin{cases} X_s = W_s + \frac{P_s - E_s}{d_s} \\ X_g = W_g + \frac{P_s - E_g}{d_g} \end{cases} \quad (6)$$

Then the soil moisture decreases under the effect of gravity. The final value of the soil moisture in both soil layers is formulated as follow:

$$\begin{cases} Y_s = \frac{X_s + W_{smax}}{2Th} - \sqrt{\left(\frac{X_s + W_{smax}}{2Th}\right)^2 - \frac{X_s W_s}{Th}} \\ Y_g = \frac{X_g + W_{gmax}}{2Th} - \sqrt{\left(\frac{X_g + W_{gmax}}{2Th}\right)^2 - \frac{X_g W_g}{Th}} \end{cases} \quad (7)$$

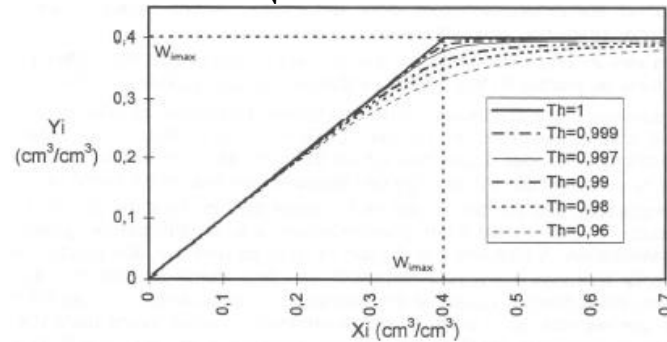


**Figure 4:** The curves of various values of the parameter  $Th$  in the Thomas model (Thomas, 1981) for the case when soil moisture is 40% (source: Cognard-Plancq, 1996 in page 97).

The parameter  $Th$  needs to be calibrated and its curvature is characterized in figure 4. The percolation leakage for each layer is obtained as follows:

$$\begin{cases} PR_s = (W_s - Y_s)d_s \\ PR_g = (W_g - Y_g)d_g \end{cases} \quad (8)$$

## 3) Calculation of ET

The calculation of ET is based on the MEP model. The ET of the bulk layer represents the total ET while the ET from the topsoil decomposes into evaporation from the bare ground and 20% of the vegetal transpiration from the work by Loumagne *et al.* (1996).  $E_g$  equals to  $ET$  obtained in equation (19) in *Appendix*. From equations (11), (14) and (19) in *Appendix*, the surface soil ET is defined as:

$$E_s = (1 - f_{veg})E_v + 0.2f_{veg}T_r \frac{W_s}{W_{smax}} \quad (9)$$

### 3.3.3. GR4H model

The GR4H model (Perrin *et al.*, 2003) is an hourly lumped rainfall-runoff model with four parameters, as shown in figure 5a. The parameters are:  $x_1$ , maximum capacity of the production store (mm);  $x_2$ , groundwater exchange coefficient (mm);  $x_3$ , maximum capacity of the routing store;  $x_4$ , base time of the unit hydrograph (hours).

In our study, the interception reservoir and the production reservoir mentioned in sections 3.3.1 and 3.3.2 will replace the corresponding parts (interception and production store) in GR4H model, as shown in figure 5b. The routing flow  $PR$  is thus the connection to the GR4H model. To adjust the time lag between rainfall and flow peak, 90% of  $PR$  is routed by the unit hydrograph UH1 and then through a non-linear routing store. The remaining flow is routed by the unit hydrograph UH2. A ground water exchange term  $F$  acts on both flow components. The outflow  $Q$  is the sum of the two routing. The interception process and the production store evolution functions in the original GR4H model are presented in *Appendix*.

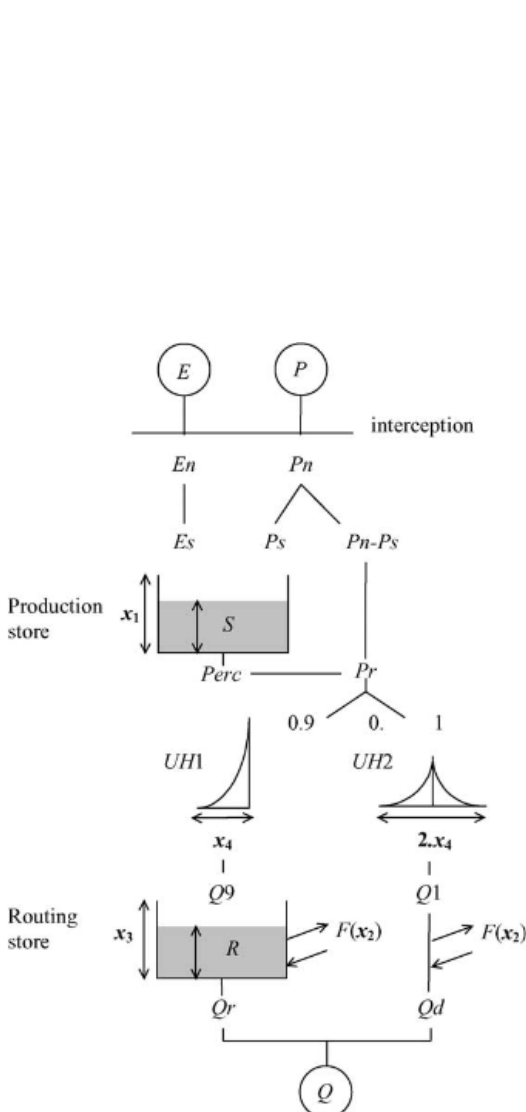


**Figure 5a:** The diagram of GR4H model (source: Perrin *et al.*, 2003 in page 3).

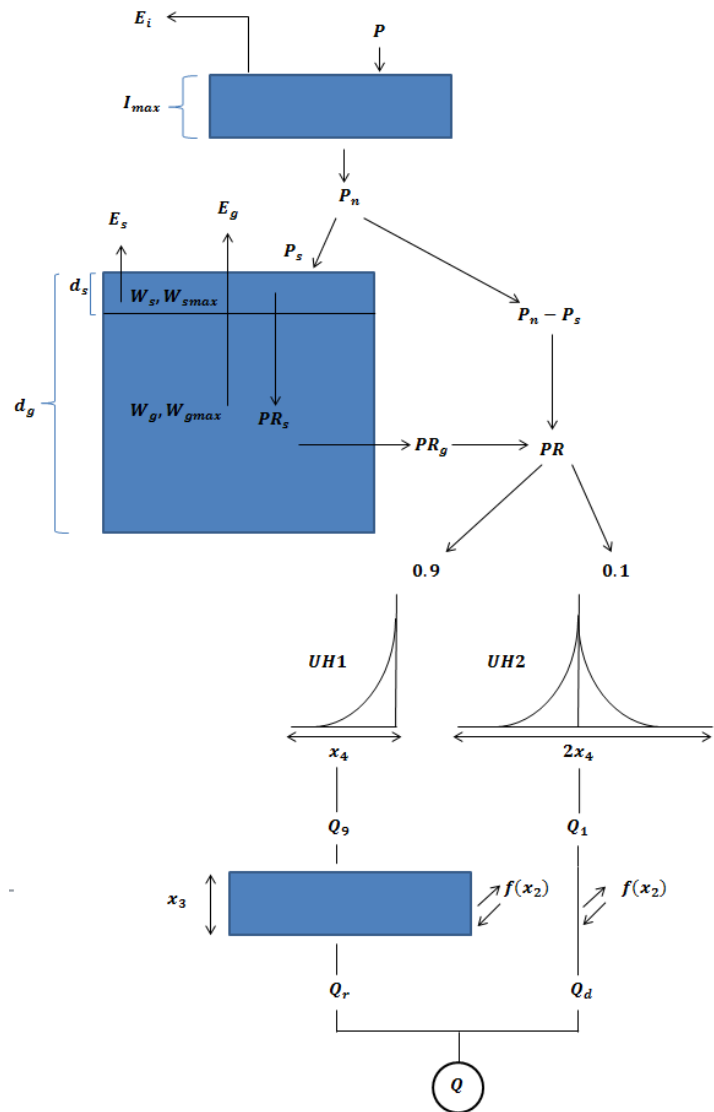


**Figure 5b:** The diagram of the modified Interception-GRHUM-GR4H model used in this study.

### 3.4. Model coupling

The MEP model and the “Interception-GRHUM” model (hereafter, I-GRHUM) are the models to be coupled, which will create the important interactions between AET and soil moisture. The approach of coupling to exchange information between models can be different: external coupling, iterative coupling and simultaneous coupling (Morita and Yen, 2000). External coupling means exchange data once per time step in both directions. In other words, results from one model are used as boundary conditions in the other model (see figure 6a). Iterative coupling means to exchange data not only once per time step, but to iterate until a certain convergence criterion is achieved (see figure 6b). Simultaneous coupling means to integrate the different processes in one equation system, which is the highest level of coupling and too difficult to implement in our case. Simultaneous coupling is thus not taken into consideration in this study.

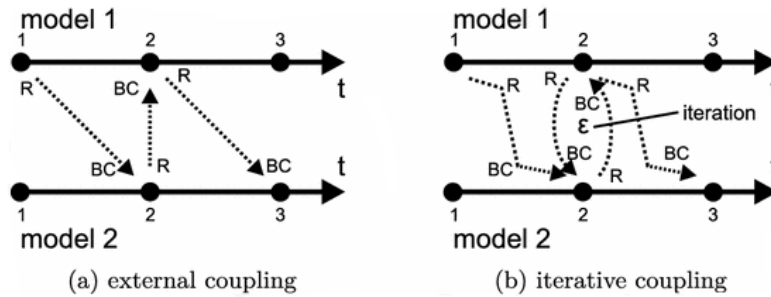


**Figure 6:** Functional principle of external coupling and iterative coupling of two models:  $R$  result,  $BC$  boundary condition,  $t$  time,  $\varepsilon$  convergence criterion (source: Becker and Burzel, 2016 in page 281).

Since our MEP-I-GRHUM coupled model depends on both water balance and energy balance, iterative coupling will be employed in our study. This approach is more stable and reduces inherent balance errors. The coupled model MEP-I-GRHUM applied with the iterative coupling method is shown in figure 7 for a given time step.

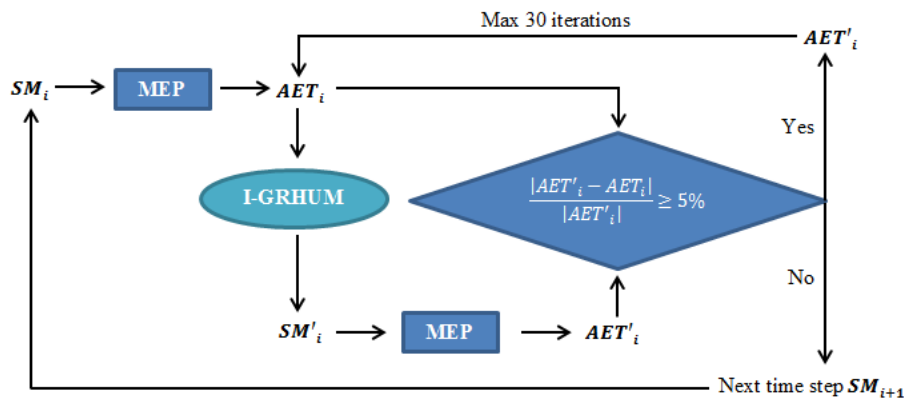


**Figure 7:** Flow chart of the iterative coupling between the MEP model and the I-GRHUM model over a time step:  $SM_i$  (%) observed soil moisture,  $SM'_i$  (%) simulated soil moisture from the I-GRHUM model,  $AET_i$  (mm) simulated AET from the MEP model with  $SM_i$  as input,  $AET'_i$  (mm) simulated AET from the MEP model with  $SM'_i$  as input.

The convergence criterion between  $AET_i$  and  $AET'_i$  aims at assimilating the information from the two models, MEP and I-GRHUM, and stabilizing the results from the coupled model. The maximum number of iterations is set to 30, in case of an endless loop. The system can thus go to the next time step when the criterion is

satisfied or at the 31<sup>st</sup> iteration. The outputs of the iterative coupling are  $SM'_i$ , which includes topsoil humidity and bulk soil humidity, and  $AET'_i$ .

Figure 8 shows how the iterative coupling is embedded in the structure of the modified GR4H model. The interaction between the soil moisture and AET can thus be connected to represent the two-way feedbacks in the real system of saturated soil and atmosphere.

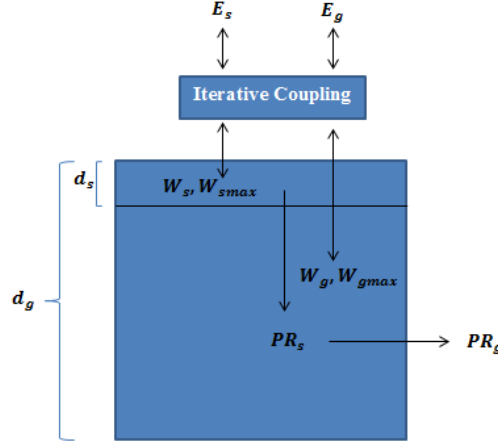


**Figure 8:** The diagram of the iterative coupling routing in the modified GR4H model.

### 3.5. Model assessment

The results of the new coupled model are evaluated by applied existing several criteria on model performance on the following target variables: AET, soil moisture and flow simulation. In our study, model modifications can be accepted only if most of the criteria of model performance are improved (or not too much degraded). A compromise must be made if significant improvements on some simulation target variables are detected at the price of a degradation of other simulation target variables.

The model performance criteria used are:

- 1) The Nash-Sutcliffe efficiency (NSE) (Nash and Sutcliffe, 1970):

$$NSE = 1 - \frac{\sum_{i=1}^N (x_{sim,i} - x_{obs,i})^2}{\sum_{i=1}^N (x_{obs,i} - \overline{x_{obs}})^2} \quad (10)$$

where  $N$  is the total number of observations,  $x_{sim,i}$  is the simulated value at time step  $i$ ,  $x_{obs,i}$  is the observed value at the same time step,  $\overline{x_{obs}}$  is the mean value of the observed data. Essentially, the closer the efficiency is to 1, the more accurate the model is.

- 2) Kling-Gupta Efficiency (KGE) (Gupta *et al.*, 2009):

$$KGE = 1 - \sqrt{(r - 1)^2 + (\alpha - 1)^2 + (\beta - 1)^2} \quad (11)$$

where  $r$ ,  $\alpha$  and  $\beta$  are the linear correlation coefficient, the ratio of the standard deviation and the ratio of the mean value respectively between observed and simulated data. The KGE reaches 1 for a perfect match between observations and the model. As a decomposition of NSE, KGE is often used as a model calibration criterion for its improved and diagnostically performance.

3) The percent bias (PB):

$$PB = \frac{|\sum_{i=1}^N (x_{sim,i} - x_{obs,i})|}{\sum_{i=1}^N x_{obs,i}} \times 100 \quad (12)$$

This criterion measures the average tendency of the simulations to be larger or smaller than the observations.

4) The rooted mean square error (RMSE):

$$RMSE = \sqrt{\frac{\sum_{i=1}^N (x_{sim,i} - x_{obs,i})^2}{N}} \quad (13)$$

This criterion characterizes the variance of the estimation error and a value of 0 indicates a perfect fit to the observations.

5) The coefficient of determination ( $R^2$ ):

$$R^2 = \left\{ \frac{\sum_{i=1}^N (x_{obs,i} - \bar{x}_{obs})(x_{sim,i} - \bar{x}_{sim})}{\sqrt{\sum_{i=1}^N (x_{obs,i} - \bar{x}_{obs})^2} \sqrt{\sum_{i=1}^N (x_{sim,i} - \bar{x}_{sim})^2}} \right\}^2 \quad (14)$$

This criterion measures how well observations are replicated by the model. The range of  $R^2$  is from 0 to 1 and the closer to 1 the more total simulated data can be explained by the model.

Note that the mathematical transformation on flow is necessary for high and low flow evaluations. From the works by Pushpalatha *et al.* (2012), a summary of the transformations on NSE criterion index is given:

- $NSE_Q$  is used to evaluate high flows and is of no use for low flow evaluation.
- $NSE_{\sqrt{Q}}$  provides a more balanced evaluation on both high and low flows.
- $NSE_{\ln Q}$  emphasizes on the low flows, like the criterion  $RMSE_{Q^{0.2}}$  from the work by Chiew *et al.* (1993).

In addition, reference high and low flow thresholds are defined in our study as the 80% ( $Q_{80\%}$ ) and 20% ( $Q_{20\%}$ ) percentiles, respectively, both estimated from long time series of flow observations. The volume of simulated flows over  $Q_{80\%}$  and the duration of simulated flows under  $Q_{20\%}$  are also regarded as criteria for model performance.

## 4. Materials

### 4.1. Study Area: Les Avenelles Catchment

With an area of 45.6 km<sup>2</sup> on the plateau of Brie, Les Avenelles is a sub-catchment located east of the Orgeval river (in the Orgeval catchment) that flows in the Seine-et-Marne department in France (see figure 9a). This catchment is an experimental catchment monitored by the Oracle team of IRSTEA since 1962. Like an isosceles triangle shape, whose geometric summit corresponds to the outlet, the catchment of Les Avenelles has a slightly differentiated topography. Influenced by the moderate oceanic climate and characterized by a hydromorphic sandy soil, the basin is regularly saturated with water and thus predominantly rural and highly anthropogenic

(Loumagne and Tallec, 2013). Table 1 summarizes the overall meteorological conditions in the Les Avenelles catchment.

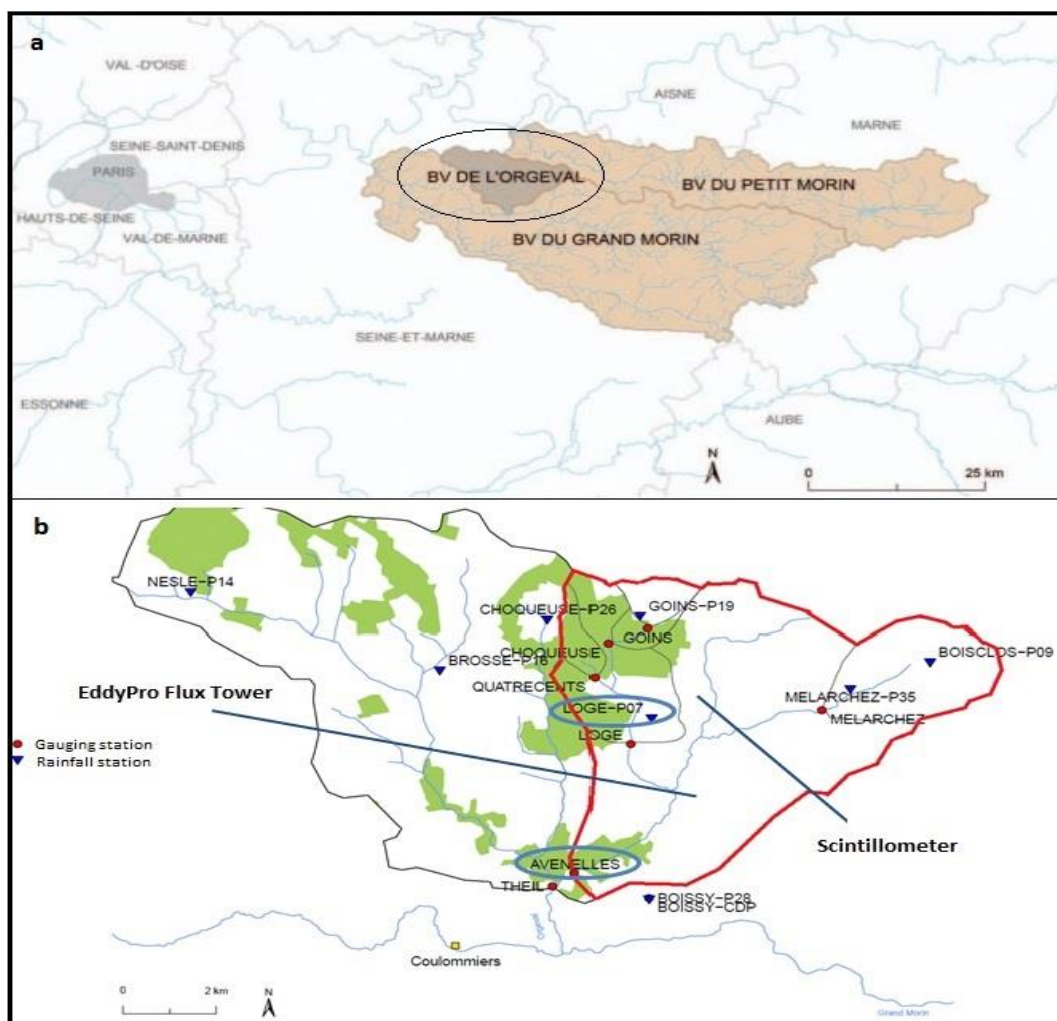


**Figure 9a.** Location of the Orgeval bassin (source: Loumagne and Tallec, 2013 in page 13). **Figure 9b.** Les Avenelles catchment (red edge) is a sub catchment of the Orgeval catchment. Gauging stations and rainfall stations are labeled in red points and blue triangles, respectively (Source: Loumagne and Tallec, 2013 in page 14).

**Table 1.** Monthly and annual meteorological averages that characterize the local climatic conditions of the Les Avenelles catchment over the period 1970-2017. Data are from the meteorological station of Boissy-le-Châtel (code: BOISSY-METEO), situated in south of the Les Avenelles catchment.

	J	F	M	A	M	J	J	A	S	O	N	D	Annual
Potential ET (mm)	14	18	41	66	85	104	114	95	64	34	15	12	662
N rainy days	19	17	15	15	16	14	13	14	17	21	20	20	201
Rain (mm)	61	53	46	52	63	56	63	59	55	66	59	76	709
Mean temperature (°C)	3	4	7	10	13	17	19	18	15	11	6	4	11
Max temperature (°C)	6	7	11	15	18	22	24	24	20	15	10	6	15
Min temperature (°C)	1	1	3	5	8	11	13	12	10	7	4	1	6
Air humidity (%)	90	86	81	77	79	80	78	78	82	88	91	91	83
Solar radiation (kJ/cm <sup>2</sup> )	0.3	0.5	1.0	1.6	1.9	2.1	2.0	1.7	1.3	0.7	0.4	0.2	1.1

This sub-catchment has recently been equipped with a flux tower and a scintillometer instrument, whose locations are indicated in figure 9b, to monitor the AET process (described in detail in the “ORE ORACLE instrumentation Report”).

## 4.2. MEP input data and AET field observations

The flux tower and the scintillometer measurements of AET are in situ measurements that are used in our study for their high quality and resolution. The input data of the MEP model are from the measurements of the flux tower and the data from the scintillometer will serve as the reference observation for the evaluation of the results of the MEP model.

The process of the flux tower data treatment is presented in figure 10. The flux tower (see photo in figure 11a) can continuously measure the ecosystem greenhouse gases flow, micro-meteorological parameters and solar radiation at hourly time steps though the bound sonic sensors mounted at 1.5m above the ground. Analyzed by EddyPro<sup>4</sup>, measurements of atmospheric exchanges are also produced in a 30-minute time resolution. However, after a preliminary data quality-control, it was observed that this measurement suffers from an energy balance problem and the AET series derived by EddyPro are not employed in our study.

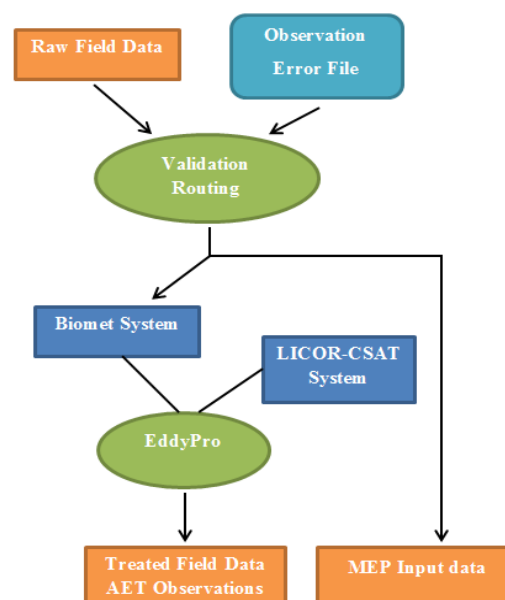


**Figure 10.** The simplified process of the flux tower field data treatment.



**Figure 11a.** The flux tower in Les Avenelles catchment (source: ORACLE instrumentation report).



**Figure 11b.** The scintillometer in Les Avenelles catchment (source: ORACLE instrumentation report).

Data from the flux tower, which are of 30-minute temporal resolution for the period from 05/2016 to 12/2017, are used as input to the MEP model. The data needed to run the MEP model are: air temperature, surface soil temperature at depth of 5 cm, specific humidity, net radiation, volumetric soil moisture at depth of 5 cm and volumetric soil moisture at depth of 75 cm. There is a missing blank of these data for

<sup>4</sup> EddyPro (<https://www.licor.com>) is the software for processing eddy covariance data.

two weeks at the end of 12/2016. As the ET process is not important in winter, we assumed that this gap of data in December year 2016 could be filled by the same weeks of the year 2017 to obtain a continuous set of data set.

Wave-physically based, the scintillometer (see photo in figure 11b) is an instrument used to detect the change in scintillation of an electromagnetic beam passing through the atmosphere as a result of the change in the refractive index of the air along its path. The scintillometer is widely accepted due to its ability to quantify the AET at landscape scale over several kilometers and to provide continuous AET measurements. The ET records of every 30 minutes by the scintillometer are chosen to validate the MEP results. The continuous scintillometer data that is available in this study is from 05/2016 to 07/2017. Thus, the period for the validation of the MEP model results is from 05/2016 to 07/2017.

### 4.3. Data for the calibration of the GR4H model

The dataset SAFRAN<sup>5</sup> provides the meteorological data needed to compute PET (see *Appendix*). It produces an analysis at the hourly time step using ground data records for an 8km×8km spatial resolution over France (see figure 12). The detailed description can be found in Vidal *et al.* (2010). We used this hourly dataset. The coordinates we used to extract the data for the Penman-Monteith PET estimation correspond to the station BOISSY-METEO. We considered the pixel of BOISSY-METEO station to be representative for the entire catchment.

Hourly precipitation and discharge time series in Les Avenelles catchment are those from the dataset BDOH-ORACLE<sup>6</sup>. In the experimental sites of ORACLE, all the hydro-meteorological elements are monitored via a complete measurement network: gauging stations at the outlet of each sub-catchment, rainfall stations as well as piezometric stations spreading over the whole study area and soil moisture stations in surface and in depth.

Therefore, in our study, Penman-Monteith PET, areal averaged precipitation (average from point rainfall data from stations available in the Les Avenelles catchment, namely, BOISCLOS-P09, GOIN-P19, LOGE-P07 and MELARCHEZ-P35, see figure 9b) and discharge data from the gauging station “Avenelles” for the period 1995-

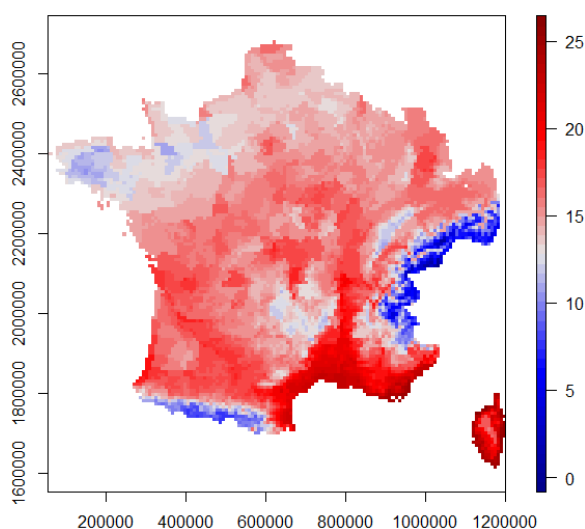


**Figure 12.** The France territory is divided into 8km×8km grids in the dataset SAFRAN (meteorological reanalysis from Météo-France). For example, this figure shows the air temperature (in °C) on 2016-08-01 at 07:00:00.

<sup>5</sup> SAFRAN is a reanalysis dataset provided by Météo-France (French national weather service, [www.meteofrance.com](http://www.meteofrance.com)).

<sup>6</sup> The meteorological and hydrological dataset (<http://data.datacite.org/10.17180/OBS.ORACLE>) is produced and managed by IRSTEA.

2005, 2005-2015 and 1995-2015 are performed to calibrate the GR4H model based on  $KGE_{\sqrt{Q}}$  criteria. The data of Les Avenelles catchment for the period from 1995-2015 are presented in figure 13. As a result of the calibration of the model for the three different periods, we obtain three series of parameters for the GR4H model. The parameters and the optimized KGE coefficients are shown in table 2. The averaged parameters will be used in the simulation processes for years 2016-2017.

**Table 2.** Calibration results of the GR4H model using Penman-Monteith potential evapotranspiration, area-averaged precipitation from rainfall stations in Les Avenelles catchment (point stations: BOISCLOS-P09, GOIN-P19, LOGE-P07 and MELARCHEZ-P35) and discharge from gauging station “Avenelles” for the period 1995-2015 and two sub-periods (1995-2005 and 2005-2015).

Period	X1[mm]	X2[mm]	X3[mm]	X4[h]	$KGE_{\sqrt{Q}}$ (%)
1995-2005	188.670	-0.114	31.187	8.180	91.28
2005-2015	200.691	-0.200	32.819	8.258	81.14
1995-2015	197.540	-0.138	31.088	8.321	87.39
Average	195.633	-0.151	31.698	8.253	-

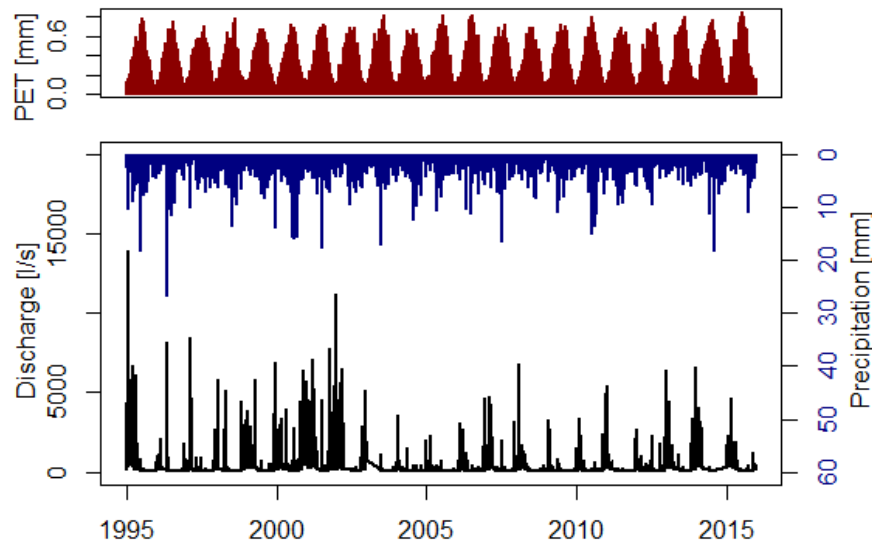


**Figure 13.** Penman-Monteith potential evapotranspiration produced from the dataset SAFRAN, averaged precipitation from the 4 rainfall stations in Les Avenelles basin and discharge from the gauging station “Avenelles” for the period 1995-2015.

#### 4.4. Normalized Difference Vegetation Index (NDVI)

The Normalized Difference Vegetation Index (NDVI) from the Moderate Resolution Imaging Spectroradiometer (MODIS), is used in this study to calculate the vegetation index to be used in the MEP model. This index is processed and produced by the NASA/Goddard Space Flight Center’s GIMMS<sup>7</sup> group. NDVI is derived from imageries processed by the NOAA Advanced Very High Resolution Radiometer (AVHRR) satellite instruments. This dataset has a temporal resolution of 8-day composite period and a spatial resolution of 250 m × 250 m grid (figure 14). To use the NDVI data in the MEP model, we abstracted the data at the geographical coordinates where the flux tower is located.

<sup>7</sup> The Global Inventory Modeling and Mapping Studies (GIMMS) are from the Global Land Cover Facility ([www.landcover.org](http://www.landcover.org)) at the University of Maryland through funding support of the Global Agricultural Monitoring project by USDA’s Foreign Agricultural Service (FAS). NDVI data is available to download at <https://gimms.gsfc.nasa.gov/download/MODIS/>

Vegetation growth is highly dependent on seasonal change while changes in short periods are rather small. We thus assumed that daily NDVI data could be reasonably acquired by the linear interpolation of raw 8-day data. Therefore, continuous daily NDVI data for years 2016 and 2017 were acquired for this study, as presented in figure 15.

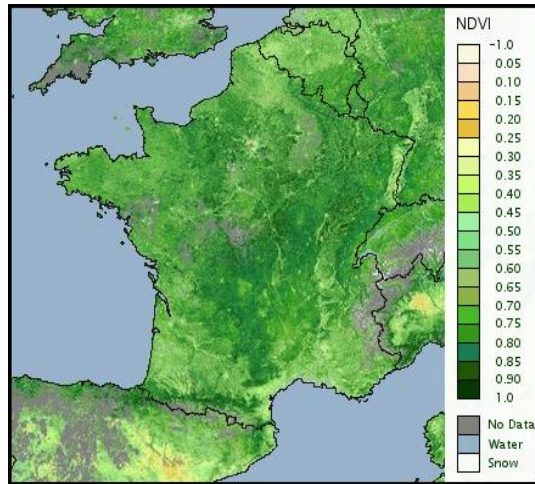


**Figure 14.** Normalized Difference Vegetation Index (NDVI) image in France for the composite period 2017/05/08-2017/05/15 processed by Terra satellite (Source from <https://glam1.gsfc.nasa.gov/>).

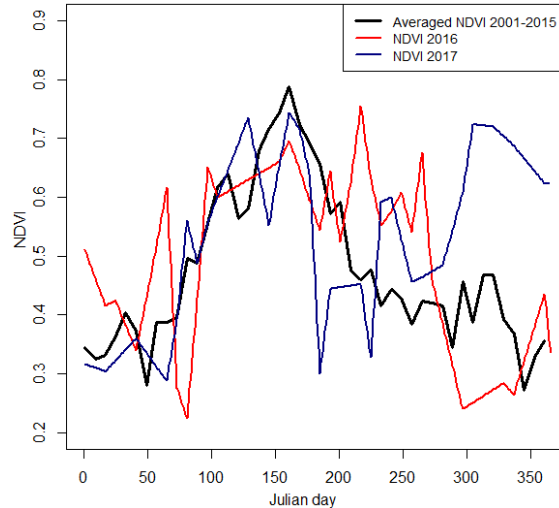


**Figure 15.** Normalized Difference Vegetation Index (NDVI) evolution in year 2016 and 2017 at the coordinate (48°51'21N, 3°10'25E) are compared with the averaged NDVI for the period 2001-2015

#### 4.5. Data Summary

In this section, a summary of the data used in this study is given in table 3.

**Table 3.** Summary of all the input data used for each part of the work and for each model used in this study.

Target Variable	Dataset/Field Data	Summarized Information	Target Model	Period
ETP	SAFRAN	Air temperature, wind speed, specific humidity and solar radiation parameters at hourly time steps	GR4H	1995-2015
AET Observation	Scintillometer	Latent heat flux (can be converted to AET by latent heat of vaporization constant) at 30-min time steps	Compare with MEP	05/2016-07/2017
AET Simulation	Flux Tower	Air, surface soil temperature, specific humidity, net radiation and soil humidity at 30-min time steps	Coupled Model & MEP	05/2016-12/2017
NDVI	MODIS	NDVI of temporal resolution of 8-day composite period	Coupled Model & MEP	05/2016-12/2017
Precipitation	BDOH-ORACLE	Precipitation representative of the Les Avenelles catchment at hourly time steps	Coupled Model & GR4H	1995-2015 & 05/2016-12/2017
Discharge	BDOH-ORACLE	Outflow of Les Avenelles catchment at hourly time steps	Coupled Model & GR4H	1995-2015 & 05/2016-12/2017

## 5. Results

### 5.1. Input data analysis

In order to verify if the MEP model is capable of simulating the AET for a longer period than the one studied in the work by Peredo (2017), the input data quality control for the period 05/2016-12/2017 was first reviewed. The quality-controlled data are: surface soil temperature, air temperature, specific humidity, net radiation, surface soil moisture and deep soil moisture. A summary of missing field data from the flux tower is shown in table 3, compiled after filling the gap of two weeks at the end of 12/2016. From this analysis, we concluded that data from the flux tower could be used as input data for the MEP model, since missing percentage of missing data is acceptable (less than 5%). The evolution of soil moisture and precipitation for the period 05/2016-12/2017 is shown in figure 16.

**Table 3.** Summary of missing values of field data from the flux tower (surface soil temperature  $T_s$  (°C), air temperature  $T_a$  (°C), specific humidity  $Q_s$  (kg/kg), net radiation  $R_n$  (W/m<sup>2</sup>), surface and deep soil moisture  $\theta_s$  (%) and  $\theta_b$  (%)).

Parameter	$T_s$	$T_a$	$Q_s$	$R_n$	$\theta_s$	$\theta_b$
Missing Values	52	45	46	245	285	-
Missing Percentage (%)	0.37	0.32	0.33	1.74	2.03	0.00

Infiltration is the process of water entering into soil from precipitation and the soil moisture is the quantity of water contained in the soil (Maidment, 1993). Normally, soil water content is expressed on a volumetric basis. The temporal evolution of soil moisture depends on the temporal variability of precipitation (for infiltration) and ET (for subtraction). As shown in figure 16, soil moisture increases during the rainfall events. The vertical infiltration is expressed as more water content in deeper soil and the bulk soil moisture is quantitatively higher than the surface soil moisture, as presented in figure 16.

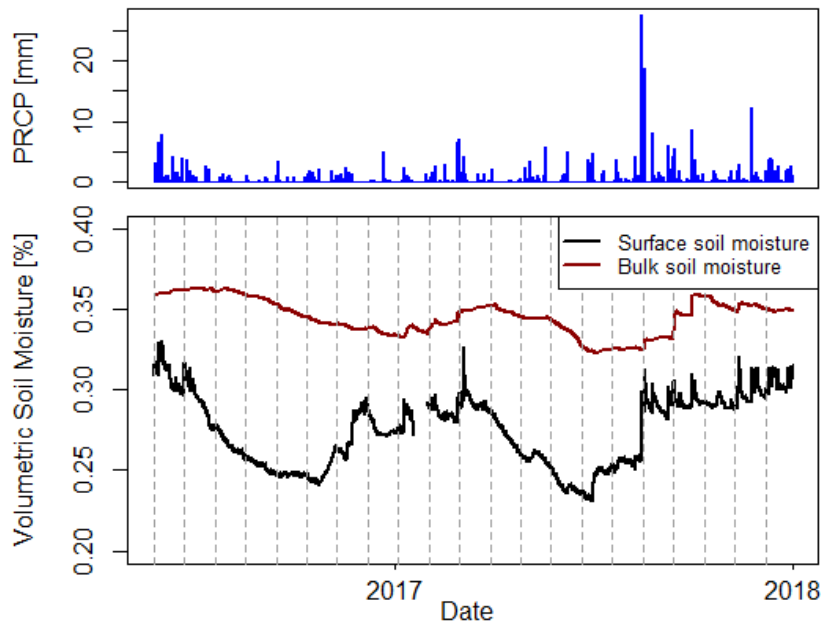


**Figure 16.** Observed precipitation (PRCP), surface soil moisture and bulk soil moisture for the period 05/2016-12/2017. Both surface and bulk soil moisture are fed by precipitation.

Figure 16 also shows that the variation of the surface soil moisture amplifies more quantitatively and shifts more frequently than the deep (bulk) soil moisture. In the vertical profiles of soil moisture, decreasing amplitude and increasing phase shift with soil depth have been observed (e.g., Wu and Dickinson, 2004). Surface water content has an immediate response to the atmospheric forcing, such as precipitation and ET, while the longer memory of soil moisture in the deeper soil layers shows their persistence in containing the water.

The evolution of temperature, specific humidity and solar net radiation for the whole study period is shown in figure 17. Specific humidity is the ratio of the mass of water vapor in a unit mass of moist air. This parameter is mainly dependent on temperature and water supply. As temperature increases, the amount of water vapor needed to reach saturation also increases as shown in figure 17.

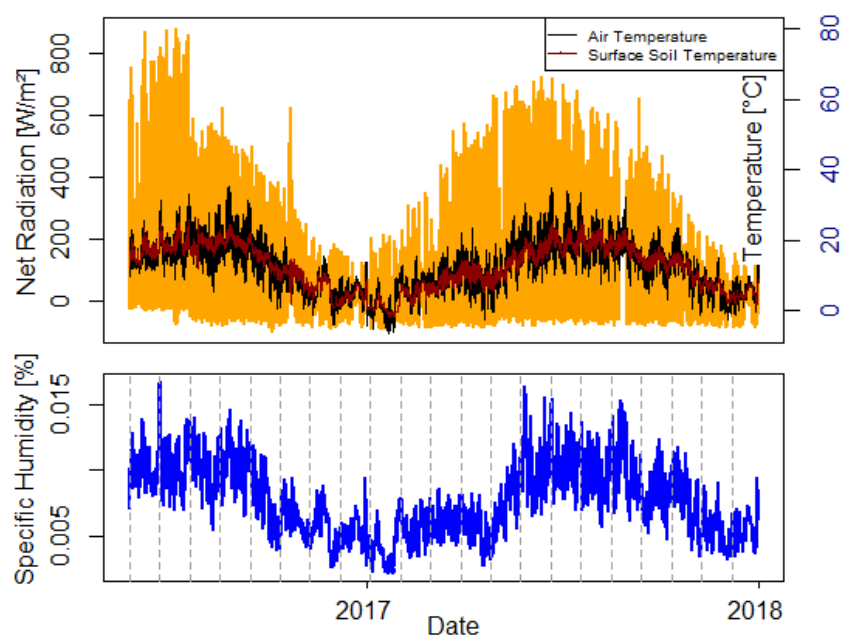


**Figure 17.** Observed data for air temperature, surface soil temperature, net radiation and specific humidity for the period 05/2016-12/2017. Solar net radiation influences the evolution of air and surface soil temperature. Specific humidity is mainly influenced by temperature.

As the only entering source of energy in the Earth system, part of the solar radiation is transformed to the augmentation of temperature in the air and the surface soil. Both air temperature and surface soil temperature follow the seasonal change of solar net radiation (figure 17) while the amplitude of the air temperature is larger than the one of the surface soil temperature due to the persistence character of the soil (Wu and Dickinson, 2004).

## 5.2. Validation of the MEP model

The time sequence chosen to validate the MEP model is from 05/2016 to 07/2017, for which the continuous scintillometer series is available. Figure 18a and figure 18b present the comparisons between the results of hourly AET from the MEP model, the AET calculated from the GR4H model (see Peredo, 2017 for details), the scintillometer field data as well as the PET series, for the period of 05/2016-07/2017. Table 4 summarizes the MEP model and the GR4H model performance values on

their ability of modeling the AET against the scintillometer field data, in terms of the NSE efficiency, PB coefficient, RMSE efficiency and  $R^2$  criterion.

**Table 4.** Performance criteria (NSE, PB, RMSE and  $R^2$ ) with respect to the hourly AET output from the MEP model and that extracted from the GR4H model.

<b>Year 2016</b> (total value from the scintillometer: 341.48mm; ETP: 494.22mm)					
	NSE	PB (%)	RMSE	$R^2$ (%)	Sum (mm)
MEP	0.654	-11.7	0.085	49.8	324.31
GR4H	0.566	-24.0	0.095	31.9	275.19
<b>Year 2017</b> (total value from the scintillometer: 475.54mm; ETP: 425.86mm)					
	NSE	PB (%)	RMSE	$R^2$ (%)	Sum (mm)
MEP	0.713	-46.7	0.104	50.6	253.74
GR4H	0.366	-49.5	0.152	20.5	244.69
<b>Year 2016-2017</b> (total value from the scintillometer: 817.02mm; ETP: 920.08mm)					
	NSE	PB (%)	RMSE	$R^2$ (%)	Sum (mm)
MEP	0.695	-32.0	0.094	47.2	578.05
GR4H	0.449	-38.8	0.126	23.4	519.88

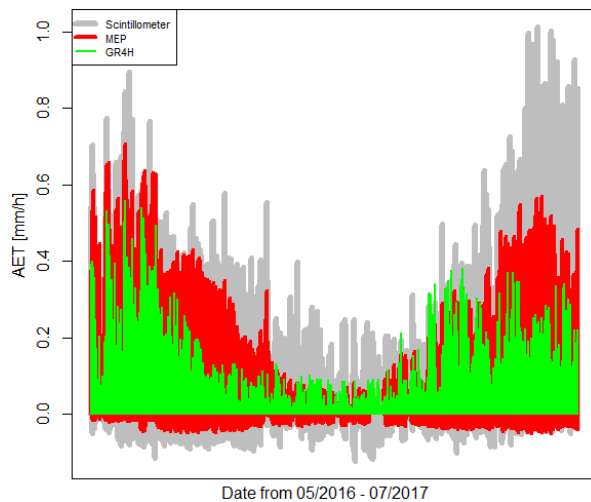


**Figure 18a.** Histogram of hourly AET of the scintillometer field data (gray), the MEP model results (red) as well as the GR4H model results (green) for the period from 2016-05-25 11:00:00 to 2017-07-16 23:00:00.

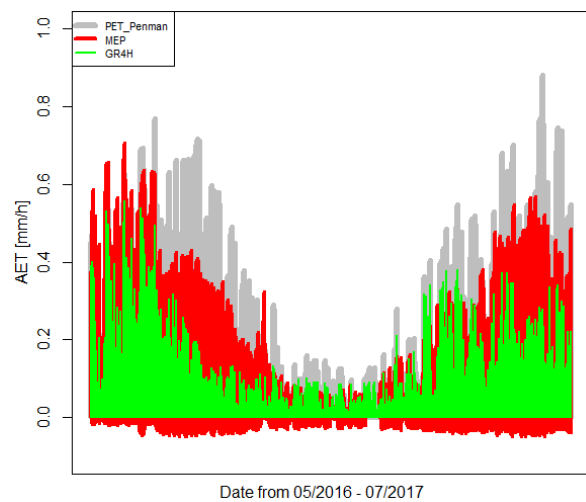


**Figure 18b.** Histogram of hourly AET of the MEP model results (red), the GR4H model results (green) as well as the Penman Monteith PET (gray) for the period from 2016-05-25 11:00:00 to 2017-07-16 23:00:00.

From the model performance summary in table 4, we can conclude that the AET simulation from the MEP model shows a better agreement to the scintillometer observations, while both the MEP and GR4H models tend to underestimate AET. This better performance for the MEP model is identified from the higher value of  $NSE$ , as well as  $R^2$ , and lower value of  $RMSE$ , compared with those for the AET extracted from the GR4H model. This tendency of underestimating AET for both models can be explained from the negative values of  $PB$ . However, the PET results from Penman Monteith formula are also lower than that from the scintillometer field data for year 2017, which suggests that the scintillometer data might be over measuring ET for the year 2017, since PET is meant to be the maximum limit of AET.

Moreover, a better representation of the seasonal evolution of AET can be seen from the MEP simulations from figure 18. Particularly, we observe that the MEP model can simulate the condensation processes, expressed as the negative values of AET, which

cannot be obtained from the GR4H simulations.

Figure 19 shows the accumulated curves of AET from the MEP and GR4H models, plotted against the accumulated curve of the scintillometer field data. The MEP model results show a better fit for the year 2016, compared with the GR4H model results, which indicates that the MEP model can quantitatively better model the AET process. The unmatched situation for the year 2017 is probably due to the overestimation obtained from the measurement provided by the scintillometer. This can be explained by the fact that the quality control treatment of these data is still in progress, and the data has not been fully validated yet. Our results are an indication that in-depth validation is still needed. This difference in the year 2017 can also be seen in table 4, where the total AET obtained from the MEP model for 05/2016-12/2016 is 324.31 mm, very close to the observed field data of 341.48 mm, and the total scintillometer field data for 01/2017-07/2017 is 475.54 mm, much higher than the PET estimation of 425.86 mm.

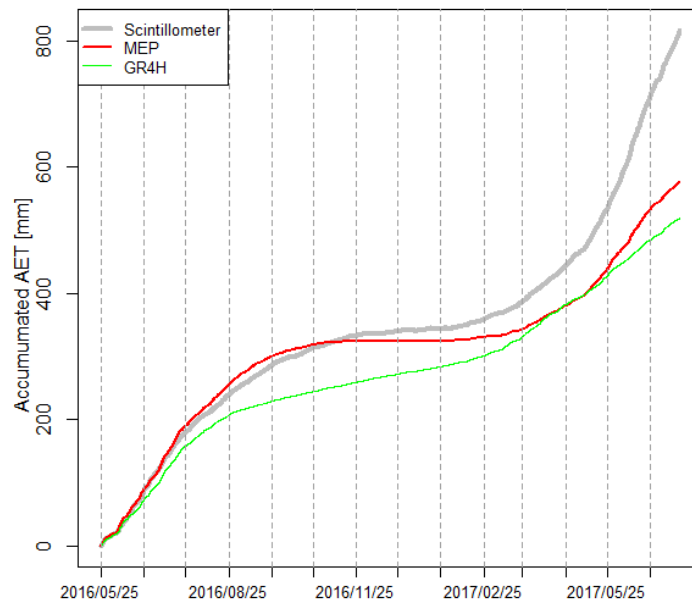


**Figure 19.** The accumulated curve of the AET series calculated by the MEP model (red), the GR4H model (green) and the scintillometer field data (gray) for 05/2016-12/2017.

Overall, compared with the AET estimation performed inside the GR4H model, which is based on the PET and the soil moisture extraction function, a better AET simulation can be obtained from the MEP model. This is not only because it follows the seasonal evolution of AET but also due to the quantitative correctness and the better model performance when simulations are evaluated against the observed data. Despite the imperfectness of the observed data from the scintillometer that was used as a benchmark, notably for the year 2017, the potential of the MEP model to produce better AET results than the GR4H model is confirmed, at least for the year 2016, which provides a possibility to integrate this MEP model in the GR4H model to increase its modeling performance.

The response of the MEP model to the resolution of its input data is also investigated. The effect of the aggregation of the input data on the MEP model is presented in figure 20. The input data are aggregated, at the time steps of: one hour, six hours,

twelve hours and one day. They are then used separately within the MEP model. The longer the aggregation period, the more the amplitude of AET variation decreases. The effect of aggregation suggests that sub-daily time scales could be too noisy to derive meaningful information from the MEP model to the water-balance framework. As such, a daily estimation from the MEP model might be better capable of resolving the noise and smoothing the inherent inaccuracy to maximize the simulation performance in the water-balance framework.

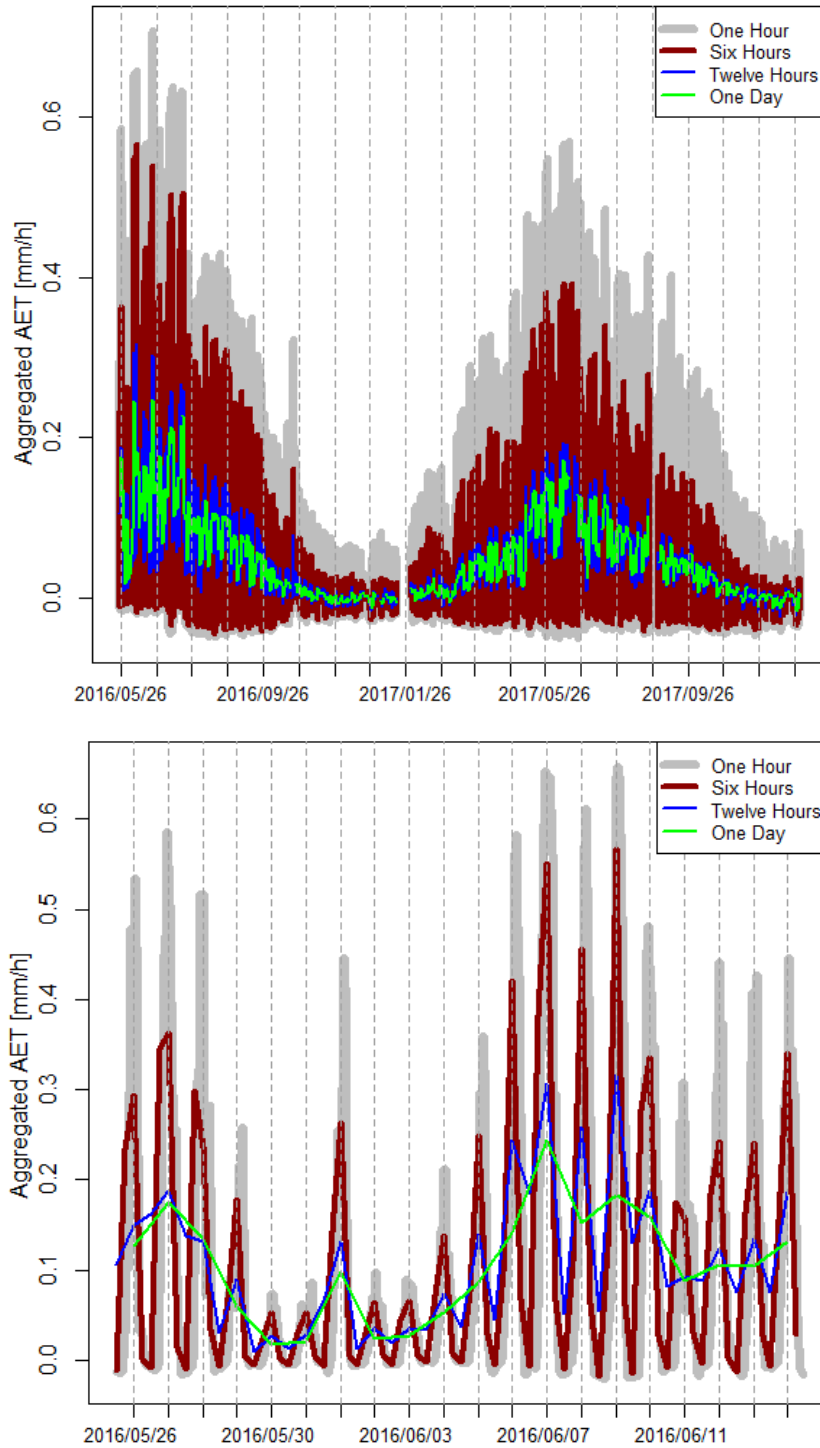


**Figure 20.** The effect of input data aggregation in the MEP model for the whole simulation period (top) and a zoom for shorter period from 26/05/2016 to 14/06/2016 (bottom).

### 5.3. MEP-GR4H modeling chain

The chain mechanism from the work of Peredo (2017), an uncoupled conjunctive modeling, was also tested within our longer study period by doing a simple exchange of input and output between the GR4H model and the MEP model. In this uncoupled approach, we consider the successive execution of the two models: the output of the MEP model, which is the simulated AET data, is used as input to the GR4H model. Therefore, a feedback from the GR4H model to the MEP model is not incorporated. The internal transformation from PET to AET in the GR4H model is also deleted and the output from the MEP model is directly incorporated in the evolution of the state of the production store in the GR4H model (figure 5a).

In order to test this chain, two sets of parameters have been derived from the calibration of the GR4H model: one from using GR4H in its original structure (without MEP) and another using the MEP-GR4H modeling chain. These two sets of parameters and their respective periods of calibration are presented in table 5. The parameter set (Param1) is obtained using the Penman-Monteith PET and it varies from the parameter set (Param2) obtained from the simulation results of the MEP-GR4H modeling chain (using AET and not PET as input). The use of different sources of forcing data in the same general hydrological framework (the GR4H structure), PET versus AET, influences the model parameterization. An improved calibration performance can be found in the MEP-GR4H chain, since the  $KGE_{\sqrt{Q}}$  criterion obtained is the highest (82.08%).

**Table 5.** Two sets of parameters tested in the MEP-GR4H chain. The first set of parameters is derived from the calibration of the GR4H model for 1995-2015 (Param1). The second set of parameters is derived from the calibration of the MEP-GR4H chain for 05/2016-12/2017 (Param2).

Set	Calibration period	X1 [mm]	X2 [mm]	X3 [mm]	X4 [h]	$KGE_{\sqrt{Q}}$ (%)
Param1	1995-2015	195.633	-0.151	31.698	8.253	76.28
Param2	05/2016-12/2017	287.553	-1.592	52.383	7.198	82.08

Due to the current lack of long series data for the MEP model, the calibrated results from the MEP-GR4H chain (Param2) can only be compared with the simulated results from the GR4H model using Param1 for the short period from 05/2016 to 12/2017 (figure 21a). Even though the MEP-GR4H chain and the original GR4H model share the same general model structure (production and routing function), the use of different sources of input data influences the model performance. The position of the simulated flow from the MEP-GR4H chain during the low flow period is relatively higher than that of the GR4H model and, in general, closer to the observations. Thus, an improvement of the stream flow estimation during the drought period is observed from the MEP-GR4H chain, compared with the original GR4H model.

The results of the simulation of the MEP-GR4H chain with the two sets of parameters presented in table 5 are shown in figure 21b. The simulations of the MEP-GR4H chain with calibrated parameters from the GR4H model (Param1) tend to overestimate the stream-flow, which suggests that the use of PET in the calibration of the GR4H model tends to result in less extraction of water from the production reservoir (comparatively to the use of AET in the calibration). This is an indication of an underestimation of AET in the water-balance framework based in the GR4H model (original structure). This is also observed from the table 4, where the sums AET in the

GR4H model for each year 2016, 2017 and for the whole period 2016-2017 are lower than the sums of AET produced from the MEP model, as well as from the field observations.

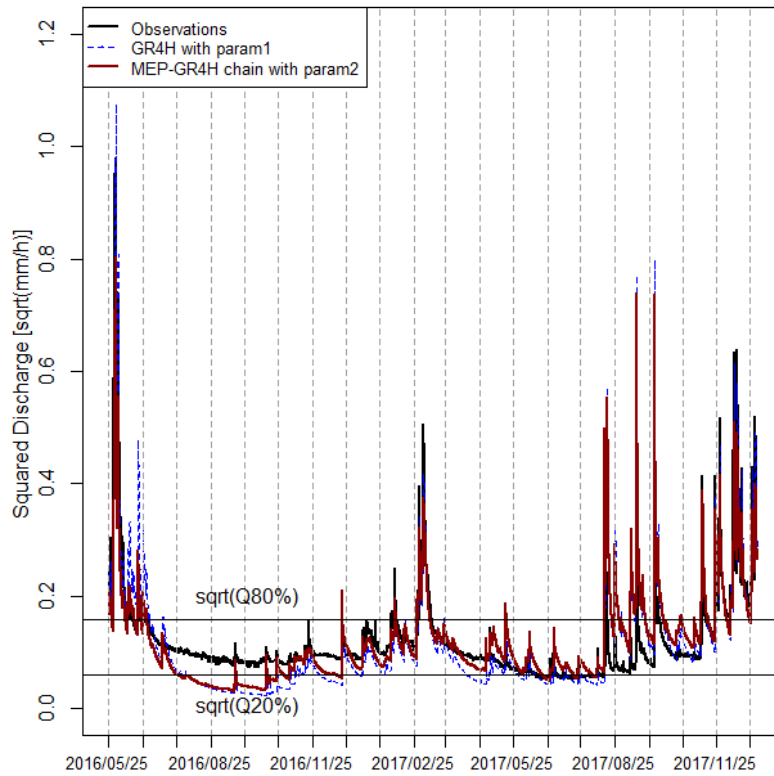


**Figure 21a.** Stream-flow simulations from the GR4H model and the MEP-GR4H chain, compared against observations for the period from 05/2016 to 12/2017.

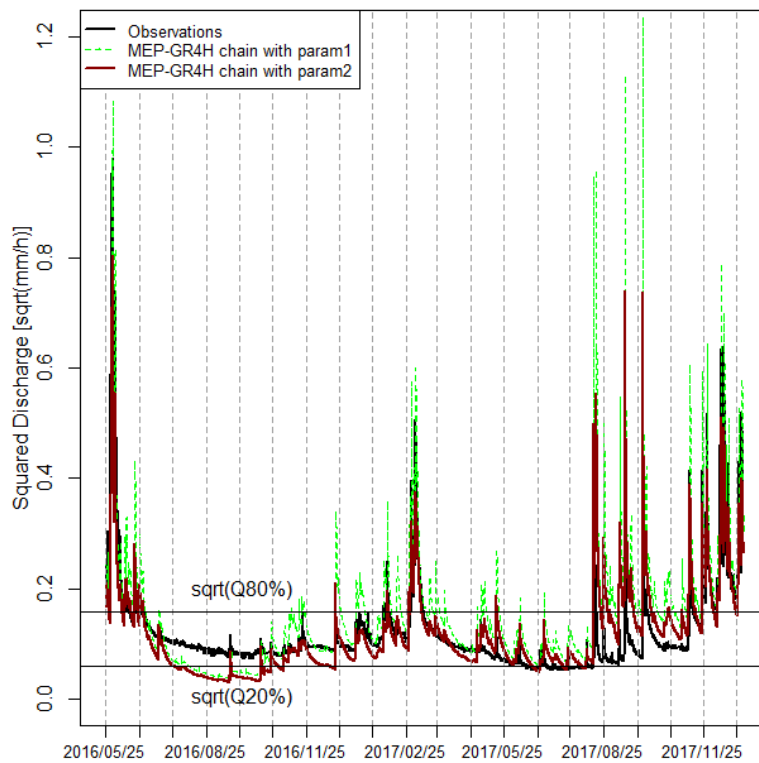


**Figure 21b.** Stream-flow simulations of the MEP-GR4H chain using different sets of parameters (see table 5) for the period from 05/2016 to 12/2017.

Table 6 summarizes the model performance criteria of the GR4H model with Param1 (blue dashed-line in figure 21a), the MEP-GR4H chain with Param1 (green dashed-line in figure 21b) and the MEP-GR4H chain with Param2 (red line in figure 21a and 21b) on high flow and low flow evaluations for 05/2016-12/2017.

**Table 6.** High and low flow evaluations on the GR4H model and the MEP-GR4H chain in terms of *NSE*, *RMSE*, *MAE*, *high flow volume* and *low flow duration*. The observed volume of the flow above the 80% threshold for 05/2016-12/2017 is 133 mm. The observed duration of the flow below the 20% threshold for 05/2016-12/2017 is 50 days.

<b>High Flow Evaluation</b>			
Model and Parameter set	$NSE_Q$ (%)	$RMSE_Q$	Volume above $Q_{80\%}$ (mm)
GR4H with Param1	79.13	0.025	168
MEP-GR4H with Param1	-0.13	0.058	303
MEP-GR4H with Param2	65.32	0.032	130
<b>Low Flow Evaluation</b>			
Model and Parameter set	$NSE_{tnQ}$ (%)	$RMSE_{Q_{0.2}}$	Duration below $Q_{20\%}$ (day)
GR4H with Param1	-27.97	0.072	213
MEP-GR4H with Param1	-9.21	0.083	68
MEP-GR4H with Param2	13.00	0.065	120
<b>Balanced Evaluation</b>			
Model and Parameter set	$R^2$ (%)	$NSE_{\sqrt{Q}}$ (%)	$MAE_Q$
GR4H with Param1	82.58	66.38	0.010
MEP-GR4H with Param1	46.02	14.45	0.019
MEP-GR4H with Param2	43.70	63.92	0.011

When forced by the results of AET from the MEP model, the MEP-GR4H chain shows an overall better performance in low flow simulation. It increases the  $NSE_{tnQ}$  criteria to 13% from the value of -27.97% produced by the GR4H model, which is driven by PET input. The evaluation of drought duration of flow below  $Q_{20\%}$  for the MEP-GR4H chain with AET input is improved from 213 days to 120 days, compared with the observed 50 days of drought duration. This improvement of low flow evaluations can thus be explained by the use of AET in the GR4H model structure. As for the high flow evaluation, the MEP-GR4H chain does not degrade much the simulations ( $NSE_{tnQ}$  values decrease from 79.13% to 65.32%) and a better estimation of the flood volume of high flows (volume above  $Q_{80\%}$ ) is found. Compared with the observed high flow volume of 133 mm, the result from the MEP-GR4H chain (130 mm) shows a better match than the 168 mm obtained from the GR4H model simulations.

These improvements of AET as forcing data indicate the potential of the MEP-GR4H chain to provide more accurate high and low flow simulations.

#### **5.4. The coupled model (MEP-I-GRHUM-GR4H)**

In the original GR4H model and in the MEP-GR4H chain, the interaction between soil moisture evolution and ET calculation is typically conducted following a one-way chain procedure, i.e., one model component acts as input and the other as response. In the fully coupled run we developed in this study, the MEP model extracts information from the two-layer production reservoir of the “Interception-GRHUM-GR4H” model (see figure 5b) and the change in the two layer pattern due to the results produced from the MEP model acts, in return, again on the MEP model. This bi-directional simulation of the interaction process is combined with a convergence criterion for the iterative coupling as shown in figure 7. This iterative approach is necessary in case

that the outputs of the coupled model get unstable and drift away from the reality.

With this increased complexity, compared with the original GR4H model, evaluations on model performance on soil moisture, AET and flow simulations are presented below.

### 1) Soil moisture evaluation

In the first place, the coupled model is calibrated against the observed surface/bulk soil moisture data from the Flux Tower to check its performance in terms of modeling soil moisture. It should be noted that this calculated soil moisture in the production reservoir of the coupled model is a simple conceptualization of the ratio between current water capacity and maximum water capacity, which is far from the physically realistic water content due to the lack of modeling persistence and time lag in the soil nature (as presented in section 5.1). Thus, a roundabout way of evaluating soil moisture is to use the relative soil moisture, which is adapted in this section to replace the soil moisture.

The observed volumetric soil moisture in depths of 5 cm and 75 cm of the Flux Tower, which here represent the soil moisture in the surface layer and the bulk layer of the soil moisture reservoir, respectively, in the two-layer soil system, can be used to calibrate the parameters  $I_{max}$  (mm),  $W_{smax}$  (%),  $W_{gmax}$  (%) and  $Th$  (-) for the period 05/2016-12/2017. These four parameters, presented in section 3.3, are: the maximum capacity of the interception reservoir, the maximum water capacity in surface layer, the maximum water capacity in the bulk layer and the Thomas parameter, respectively. In this study, this global parameterization was performed based on Differential Evolution algorithm (Ardia *et al.*, 2011).

Hence, two sets of parameters can be obtained on the basis of the observed surface and bulk soil moisture (table 7). The surface soil shows a better calibration result due to the fact that water stored at the surface has an immediate response to the atmospheric forcing, while the deeper soil has a longer memory (persistence) and this quick response can be approximated to a reservoir model.

**Table 7.** Two sets of parameters of  $I_{max}$  (mm),  $W_{smax}$  (%),  $W_{gmax}$  (%) and  $Th$  (-) derived from the global parameterization on the basis of observed surface and bulk soil moisture for 05/2016-12/2017.

<b>Calibration against observed surface soil moisture</b>				
$I_{max}$ (mm)	$W_{smax}$ (%)	$W_{gmax}$ (%)	$Th$ (-)	$KGE$ (%)
0.40	0.6728	0.3739	0.9996	84.27
<b>Calibration against observed bulk soil moisture</b>				
$I_{max}$ (mm)	$W_{smax}$ (%)	$W_{gmax}$ (%)	$Th$ (-)	$KGE$ (%)
0.01	0.8909	0.7253	0.9984	37.90

The two sets of parameters are used separately to simulate both the surface and bulk soil moisture for period from 05/2016 to 12/2017 and then the result of the bulk soil moisture in the coupled model is compared with that in the production reservoir in the GR4H model. The soil moisture simulated from the GR4H model for the same period is calculated from the averaged parameters in table 2.

Table 8 represents the performance criteria in terms of RMSE efficiency, Pearson's correlation coefficient,  $R^2$  criterion and KGE efficiency. In general, the bulk soil moisture in the coupled model shows a better performance than that in the production reservoir of the GR4H model. The correlation test,  $R^2$  criterion and KGE efficiency of the bulk soil moisture in the coupled model have greater values.

In addition, the surface soil moisture in the coupled model outstands by showing a very good performance. This good performance in the modeling of surface soil moisture (quick response layer) suggests the validity of the atmosphere-soil system incorporated within the MEP model, which subtract water from the surface layer, and the Thomas model, which drains away water from this layer.

The soil nature changes with the depth and the weaker performance of the bulk soil moisture might be ascribed to this. The progress of water flux in the two-layer production reservoir in the coupled model also points out to the possibility of integrating several soil layers to provide more detailed information. However, the key factor remains to well model the persistence and the time lag in the deeper soil layer.

**Table 8.** Performance criteria (RMSE, Pearson's Correlation,  $R^2$  and KGE) of the surface soil moisture in the coupled model, the bulk soil moisture in the coupled model and the soil moisture in the production reservoir of the GR4H model for 05/2016-12/2017. The soil moisture in the GR4H model is derived using the averaged parameters in table 2.

<b>Simulation based on the parameters from the calibration of the surface soil moisture</b>				
	<i>RMSE</i>	<i>Correlation (%)</i>	<i>R<sup>2</sup> (%)</i>	<i>KGE (%)</i>
Surface	0.1247	84.45	68.21	84.27
Bulk	0.3550	51.95	14.29	32.80
GR4H	0.3178	33.77	8.39	31.52
<b>Simulation based on the parameters from the calibration of the bulk soil moisture</b>				
	<i>RMSE</i>	<i>Correlation (%)</i>	<i>R<sup>2</sup> (%)</i>	<i>KGE (%)</i>
Surface	0.1548	73.32	46.02	65.14
Bulk	0.3121	46.45	14.03	37.90
GR4H	0.3178	33.77	8.39	31.52

Figure 22a and figure 22b present the simulations of relative soil moisture from the coupled model, based on the parameters from the calibration using the observed surface soil moisture. We present the simulations for surface soil moisture and bulk soil moisture, respectively, for the period 05/2016-12/2017. Figure 23a and figure 23b presents the simulations of relative soil moisture from the coupled model, based on the parameters from the calibration using the observed bulk soil moisture. Again, we present the simulations for surface soil moisture and bulk soil moisture, respectively, for the same period 05/2016-12/2017.

From figure 22a/b and figure 23a/b, we can see that the simulation of surface soil moisture in the coupled model shows a better match to the observed data than the simulation of bulk soil moisture. This indicates that the current model structure (reservoir model in the coupled model and the original GR4H model) might be less capable in simulating the global soil moisture (including in deeper layers).

Overall, the two-layer system in the coupled model can provide a more detailed water flux evolution in the production reservoir, compared with the original GR4H model. The coupled model also shows a better performance in modeling soil moisture.

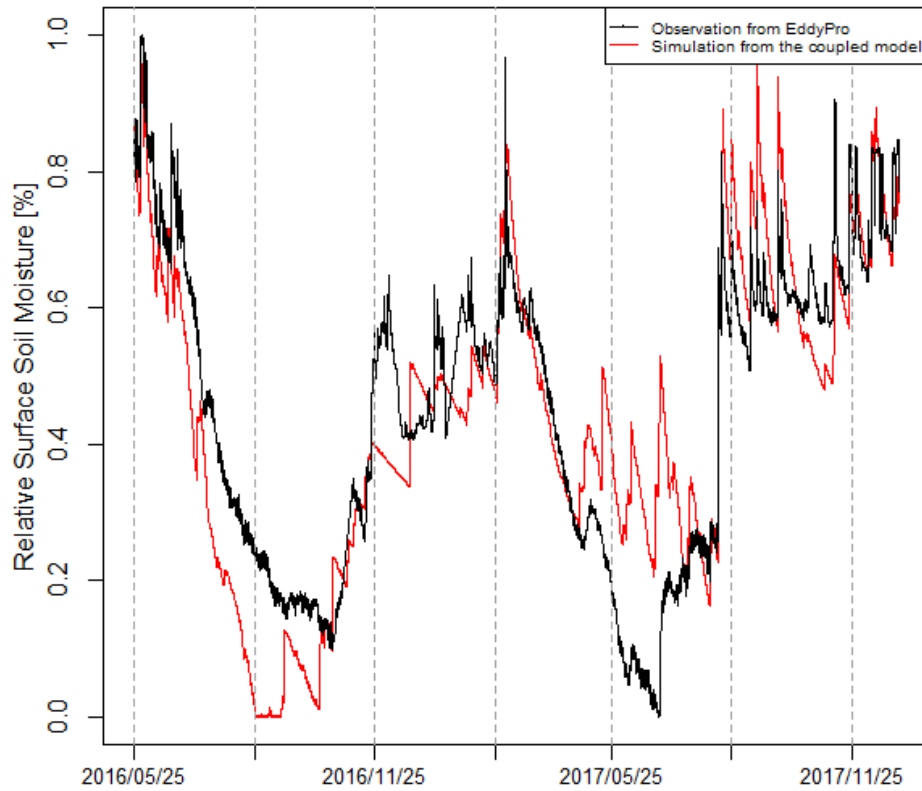


**Figure 22a.** Surface soil moisture simulation of the coupled model for 05/2016-12/2017 based on the parameters calibrated using the observed surface soil moisture.

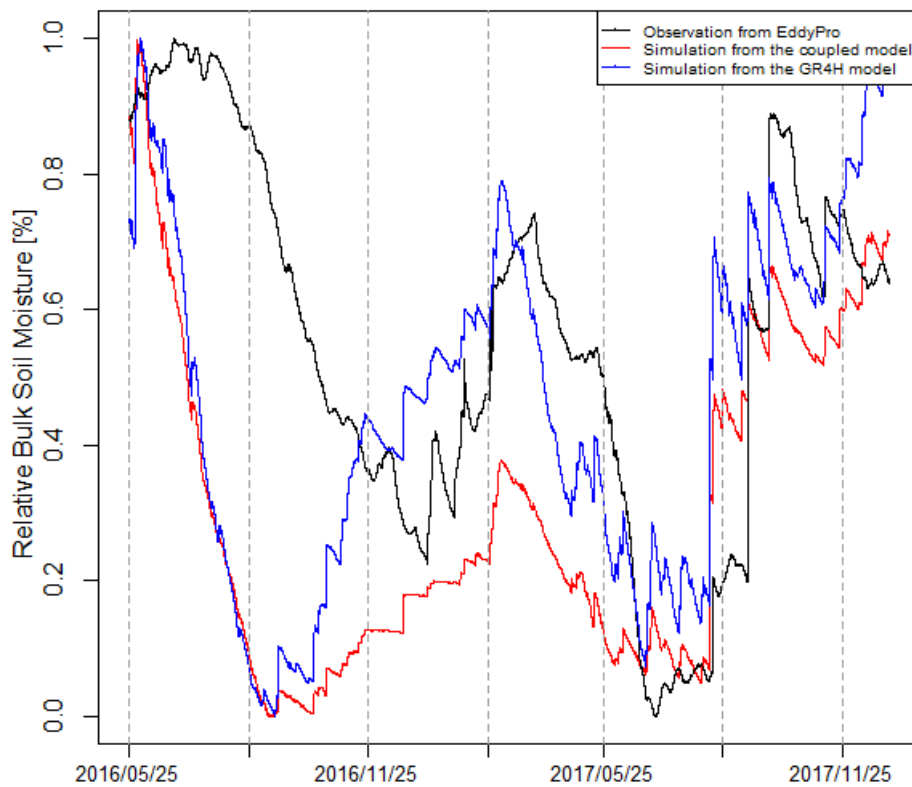


**Figure 22b.** Bulk soil moisture simulation of the coupled model for 05/2016-12/2017 based on the parameters calibrated using the observed surface soil moisture. The soil moisture simulation in the GR4H model for 05/2016-12/2017 is also presented.

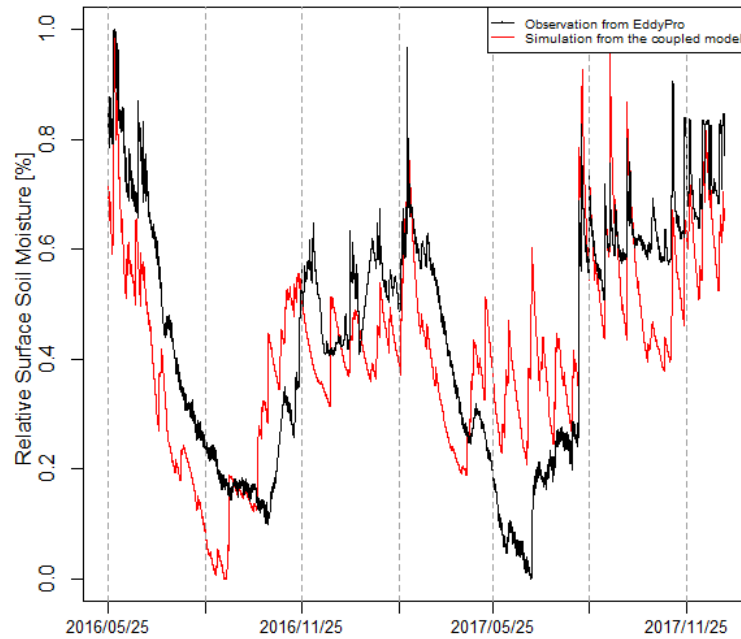


**Figure 23a.** Surface soil moisture simulation of the coupled model for 05/2016-12/2017 based on the parameters calibrated using the observed bulk soil moisture.

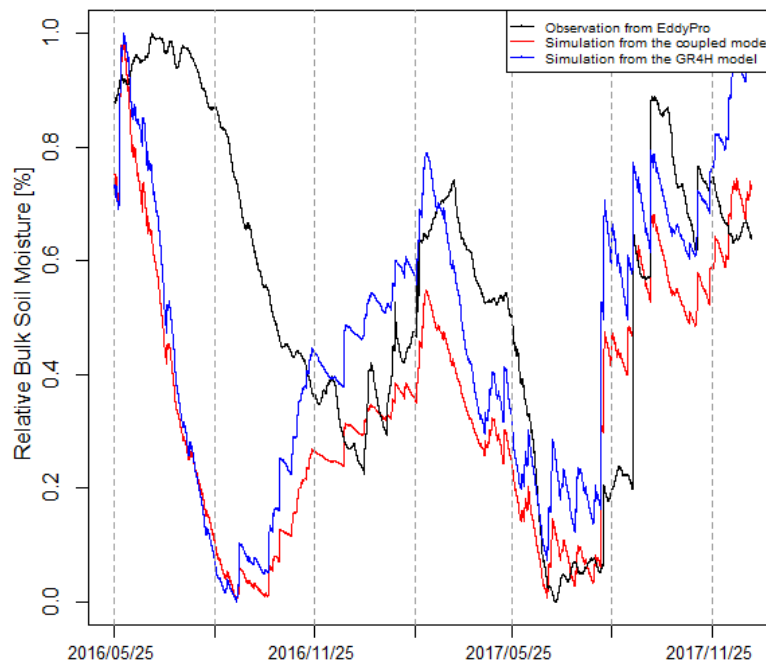


**Figure 23b.** Bulk soil moisture simulation of the coupled model for 05/2016-12/2017 based on the parameters calibrated using the observed bulk soil moisture. The soil moisture simulation in the GR4H model for 05/2016-12/2017 is also presented.

## 2) AET evaluation

In the atmosphere-vegetation-soil interactions of the coupled model, part of precipitation is intercepted by a reservoir at the top of the coupled model structure, which allows temporarily storing a small amount of rainfall. The stored water evaporates at the actual rate produced by the MEP model. The exceeded rainfall from the interception reservoir infiltrates in the two-layer production reservoir of the coupled model, where the process of ET in the bulk soil (including ET in the surface

soil) takes place.

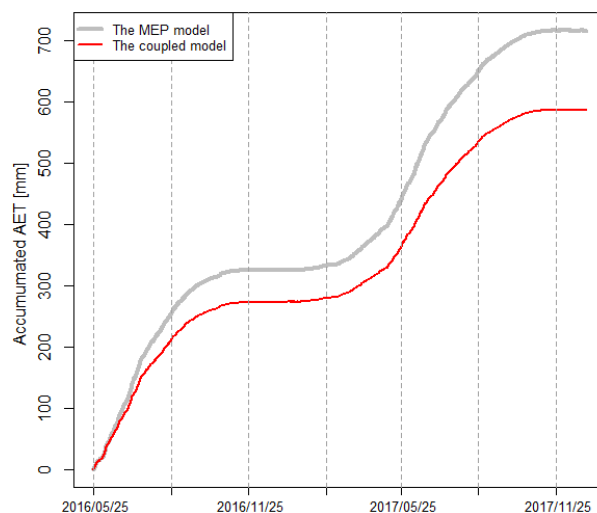
It is thus also interesting to evaluate the performance of the coupled model in modeling AET, which is presented hereafter. Whether the energy-balance MEP model still remains energy-closed in the coupled model is also examined. The simulation parameters obtained from the calibration against the observed surface soil moisture (table 7) are used to investigate the model performance and the energy conservation.

Table 9 presents the energy balance (expressed in water quantity) in the ET process of the coupled model. The transformation from energy to water quantity can be understood as follow: the energy needed to evaporate water is equivalent to the amount of water that is evaporated by this energy. In the coupled model, the total energy in the system is divided in two parts: one used to evaporate the intercepted water and the other used to carry out the ET process in the bulk soil. The sum of these two parts for the 05/2016-12/2017 study period is 595.02 mm, which gives an error of 1.35% when comparing this sum with the total energy. This means that we can consider the system as an energy-closed system.

**Table 9.** Energy balance in the coupled model for the 05/2016-12/2017 study period. Ei is the evaporation from the interception reservoir, Eg the ET from the bulk soil, Sum the sum of Ei and Eg, Ett the total ET from the coupled model and  $\Delta$  the error between Sum and Ett.

Period	Ei (mm)	Eg (mm)	Sum (mm)	Ett (mm)	$\Delta$ (%)
05/2016-12/2017	37.32	557.70	595.02	587.11	1.35

The AET simulation of the coupled model is based on the MEP model whose structure is embedded in the two-layer system in the production reservoir. From the analysis of table 9, the coupled model maintains the energy-balanced character originated from the MEP model. However, the AET simulation of the coupled model is found to drift away from the MEP model simulation (figure 24).



**Figure 24.** The accumulated AET curves between the coupled and MEP model are presented.

The total AET simulated from the MEP model for the period 05/2016-12/2017 is 716.42 mm, which is greater than that from the coupled model (595.02 mm). This deviation can be explained by the different soil moisture input to the MEP and the coupled models: the soil moisture used in the MEP model is the observed data while

the simulated soil moisture is used in the coupled model to produce AET. Even though a convergence criterion (figure 7) was introduced in the model coupling process to stabilize the iterative coupling, the divergency could not be avoided, probably due to the weak simulation of the soil moisture in the bulk soil.

Overall, the AET simulation of the coupled model can be considered satisfactory, given the limits of a good representation of the soil moisture in the bulk soil. This result indicates that the two-layer system might not be capable enough to represent the evolution of soil moisture in the whole bulk. Still, energy remains closed in the coupled model.

### 3) Stream-flow evaluation

The fully coupled model allows modeling the complete regional water cycle, from the top of the atmosphere, via the land surface and the bulk soil, till the outflow of the catchment. The energy-balance model, the MEP model, is coupled in the water-balance framework. Whether the energy-closed MEP model can provide robust estimations in a water-balance framework and whether the water balance can still be acquired in the coupled model are investigated here.

To achieve the calibration of both soil moisture and stream flow at the same time, the calibrated results presented in section 1 are used here. Since the parameters calibrated against the observed surface soil moisture show a better performance, the results with these parameters from the two-layer system production store are adapted to be used as input to the routing store in the GR4H model and to calibrate the remaining parameters (X2, X3, X4) for the study period from 05/2016 to 12/2017. Table 10 presents the final set of parameters of the coupled model. Table 11 summarizes the performance criteria of the coupled model when it runs with the parameters presented in table 10. Performance is evaluated on high flows and low flows for the period 05/2016-12/2017.

**Table 10.** The set of parameters of the coupled model for the period 05/2016-12/2017.

$I_{max}$ (mm)	$W_{smax}$ (%)	$W_{gmax}$ (%)	$Th$ (-)	$x_2$ (mm)	$x_3$ (mm)	$x_4$ (mm)	KGE (%)
0.40	0.6728	0.3739	0.9996	0.11	13.13	8.44	71.51

**Table 11.** High and low flow evaluations on the coupled model and the GR4H model in terms of *NSE*, *RMSE*, *MAE*, *high flow volume* and *low flow duration*. The observed volume of the flow above the 80% threshold for 05/2016-12/2017 is 133 mm. The observed duration of the flow below the 20% threshold for 05/2016-12/2017 is 50 days.

<b>High Flow Evaluation</b>			
Model	$NSE_Q$ (%)	$RMSE_Q$	Volume (mm)
The coupled model	71.04	0.029	152/133
The GR4H model	79.13	0.025	168/133
<b>Low Flow Evaluation</b>			
Model	$NSE_{tnQ}$ (%)	$RMSE_{Q^{0.2}}$	Duration (day)
The coupled model	-82.97	0.091	236/50
The GR4H model	-27.97	0.072	213/50
<b>Balance Evaluation</b>			
Model	$R^2$ (%)	$NSE_{\sqrt{Q}}$ (%)	$MAE_Q$
The coupled model	50.46	41.62	0.014
The GR4H model	82.58	66.38	0.010

From the criteria values shown in table 11, the coupled model does not outperform the original GR4H model. However, it also does not degrade much the simulations, compared with the original GR4H model, especially when considering the high flows. Figure 25 presents the simulation results of the coupled and the GR4H models for the study period (05/2016-12/2017). Despite the lower general performance, the energy-balance model MEP incorporated in the water-balanced framework (the coupled model) can still show relatively good simulations of high and low flows. The results point out the potential of incorporating the energy-balance model in water-balance framework, although further studies are still needed to try to improve the performance of the coupled model in terms of stream-flow simulation.

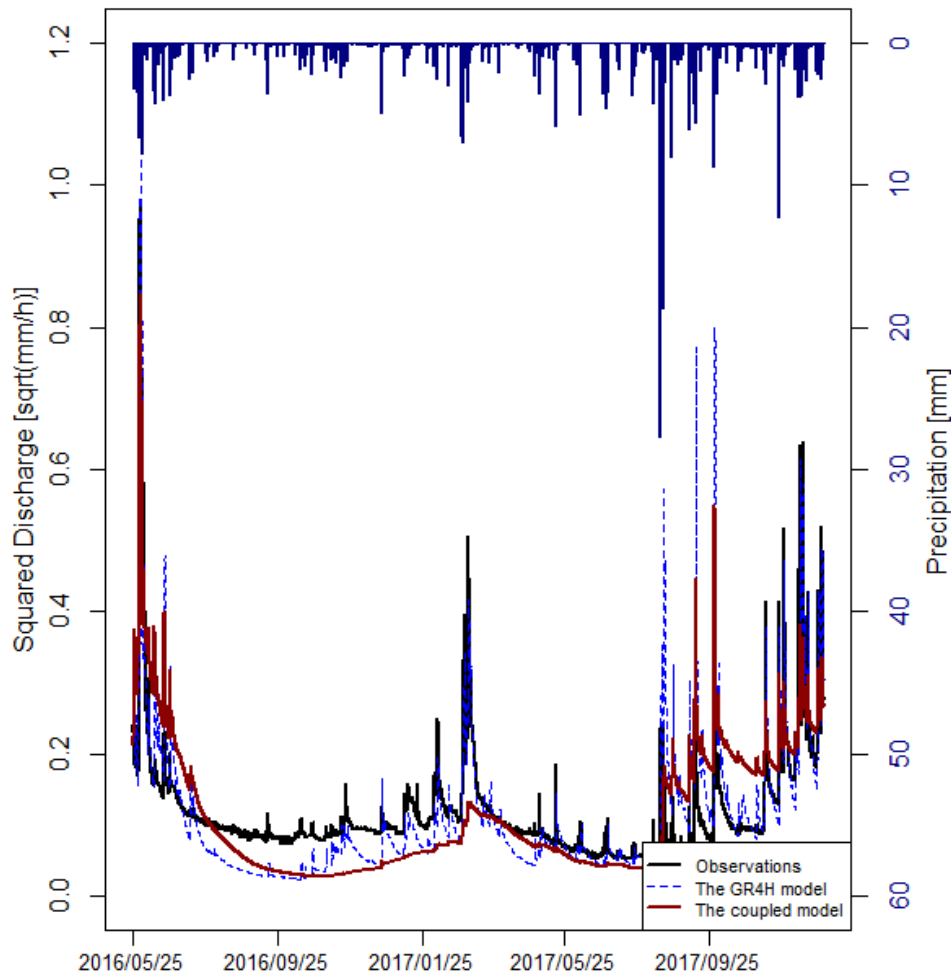


**Figure 25.** Discharge simulations of the coupled model (red line), compared with the GR4H model (dotted blue line).

Since the coupled model has the potential to produce acceptable flow simulations, an evaluation of the water balance is presented in table 12.

**Table 12.** Water balance sheet in the GR4H and coupled model for 05/2016 – 12/2017 (P, precipitation in mm; Q, simulated outflow in mm; E, actual evapotranspiration in mm; S, soil water content change in mm; X, groundwater exchange in mm; R, flow routing change in mm). Note that the sum of the observed outflow is 298.07 mm.

P (mm)	Q (mm)	E (mm)	S (mm)	X (mm)	R (mm)	$\Delta$ (mm)
+1124.33	-308.65	-743.03	-31.80	-39.89	-0.99	-0.03
+1124.33	-303.14	-587.11	-32.43	+63.74	-0.42	+264.97

We can see that the coupled model does not make full use of the water precipitated and the water budget is not closed (a quantity of 267.97 mm remains available). It seems this amount of water is consumed in the inherent convergence of the iterative coupling during each coupling run. One possible way to reduce the water wasted in this part of the modeling framework, and the inherent error it creates, could be to reduce the time step of the coupling run. The hourly time step might amplify the error and a daily time step might be necessary to smooth the inherent inaccuracy. This can also be seen from the effect of aggregation of the MEP model shown in figure 20.

Overall, the coupled model shows a relatively acceptable performance in stream flow simulation. Whether additional improvements to the energy-balance model incorporated in the water-balance framework can enhance the water (mass) conservation results needs however further investigation. It would be interesting, for instance, to simulate with longer time step to reduce the inherent error or to change the implementation of the coupling technique.

## **6. Discussion and Conclusion**

Two aspects are investigated in this study: one, what is the impact of the straightforward use of AET input on hydrological modeling, avoiding the use of PET; the other, whether and how an energy-balance model can be coupled with a water-balance hydrological model.

When forced by AET, the hydrological model GR4H performs relatively better than when the model is driven by PET input. Hence, the first question is answered: the straightforward use of AET can provide better results in hydrological modeling as it reduces the input uncertainties. As for the second aspect, our method was to build a new model based on the original GR4H model. Our goal was to replace the GR4H production reservoir with the two-layer model GRHUM, so that the energy-balance model MEP could be incorporated into the system through model coupling. Besides, an interception reservoir was added on the top of the system to represent the whole water flux in the vegetation-atmosphere-soil interactions. The coupled model system allows modeling the complete water cycle of the catchment and the simulations obtained were of quite acceptable performance. Hence, an energy-balance model can be coupled with a hydrological model and provide useful information for the modeling framework.

However, during the integration of the MEP model and the hydrological models used in this study, we have been confronted with a major disadvantage, which is the fact that their respective approaches are not of the same nature. The MEP model is semi-physical and the two-layer system (GRHUM) relies on a simplified physical approach, while the new coupled model is also based on a lumped and conceptual hydrological model (GR4H), which does not involve any measureable physical relationship. For this reason, an iterative coupling method was implemented in our study to make the models more compatible.

Even though the coupled model can provide acceptable simulation results, the water balance is found to break. An inherent error, which loses water in the convergence criterion, seems to be the main cause of this non-closure of the water balance. This

may be related to the second difficulty we have been confronted with, which is that the AET produced in the coupled model drifted away from the original MEP model, which might indicate a weak connection between the models.

Further studies are thus needed to pursue the investigations. Firstly it would be interesting to test the use of a longer time step at each run in the iterative coupling as it can smooth the noise of simulated data. Also, the pattern of the coupling mechanism could be enhanced to reduce this unbalanced chaos and to stabilize the effects of divergency.

Given that the coupled model has the advantage of simulating two more outputs, the surface/bulk soil moisture and the AET, the slight decrease of the numerical criteria for the performance of the flow simulation by the coupled model does not call into questioning the interest of this coupled model and the utility of the modifications of the production function introduced for the first time in this study. Still, more investigation is needed in order to better understand the feasibility of the energy-balance model coupled with a water-balance framework.

## References

- Andreassian V, Perrin C, Michel C, 2004. Impact of imperfect potential evapotranspiration knowledge on the efficiency and parameters of watershed models. *Journal of Hydrology*, 286(1-4):19-35.
- Ardia, D., Boudt, K., Carl, P., Mullen, K.M., Peterson, B.G. (2011) *Differential Evolution with DEoptim. An Application to Non-Convex Portfolio Optimization*. The R Journal, 3(1), 27-34. URL [https://journal.r-project.org/archive/2011-1/RJournal\\_2011-1\\_Ardia-et-al.pdf](https://journal.r-project.org/archive/2011-1/RJournal_2011-1_Ardia-et-al.pdf).
- Arya, S.P., 1988: *Introduction to micrometeorology*, 307 pp., Academic, New York.
- Bai, P., Liu, X.M., Yang, T.T., Li, F.D., Liang, K., Hu, S.S. and Liu, C.M. Assessment of the influences of different potential evapotranspiration inputs on the performance of monthly hydrological models under different climatic conditions: *Journal of Hydrometeorology*, 2259-2274, 17-8. Doi: 10.1175/JHM-D-15-0202.1.
- Bartholomeus, B.P., Stagge, J.H., Tallaksen, L.M. and Witte, J.P.M. Sensitivity of potential evaporation estimates to 100 years of climate variability: *Hydrol. Earth Syst. Sci.*, 19, 997-1004, 2015. Doi: 10.5194/hess-19-997-2015.
- Becker, B. and Burzel, A. (2016) *Model Coupling with OpenMI Introduction of Basic Concepts*. In: Setola R., Rosato V., Kyriakides E., Rome E. (eds) *Managing the Complexity of Critical Infrastructures*. *Studies in Systems, Decision and Control*, vol 90. Springer, Cham
- Bennett, W.B., Wang, J.F., and Bras, R.L., 2008. Estimation of global ground heat flux: *Journal of hydrometeorology*. Volume 9, doi: 10.1175/2008JHM940.1.
- Bhatt, U.S., Walker, D.A., Raynolds, M.K., Comiso, J.C., Epstein, H.E., Jia, G., Gens, R., Pinzon, J.E., Tucker, C.J., Tweedie, C.E. and Webber, P.J. 2010. Circumpolar Arctic Tundra Vegetation Change is Linked to Sea Ice Decline. *Earth Interactions*, 14.
- Bouchet, R.J., 1963. Evapotranspiration réelle et potentielle – signification climatique. In *Symposium on Surface Waters*. IAHS Publication No. 62. IAHS Press: Wallingford; 134-142.
- Bowen, I.S., 1926: The ratio of heat losses by conduction and by evaporation from any water surface. *Physical Review*, 27, pp 779-787.
- Brutsaert, W., 1982. *Evaporation into the Atmosphere: Theory, History, and Application*. Dordrecht, Holland. Published by D. Reidel Publishing Company. P214.
- Brutsaert, W & Parlange, M. (1998). Hydrologic Cycle Explains the Evaporation Paradox. *Nature*, 396. 10.1038/23845.
- Chen, J.M., Chen, X.Y., Ju, W.M., and Geng, X.Y. 2005. Distributed hydrological model for mapping evapotranspiration using remote sensing inputs. *Journal of Hydrology* 305 (2005) 15-39.
- Chiew, F.H.S, Stewardson, M.J., and McMahon, T.A. 1993. Comparison of six rainfall-runoff modelling approaches. *J. Hyrol.* 147, 1-36
- Cognard-Plancq, A.L. (1996). *Suivi de l'état hydrique des sols par télédétection spatiale (radar et thermographie infrarouge) et modélisation hydrologique à l'échelle du bassin versant*. PHD thesis, Université de Paris-Sud (Orsay), Cemagref (Antony), 130 p.
- Coron, L., Thirel, G., Delaigue, O., Perrin, C. and Andréassian, V. (2017). The Suite of Lumped GR Hydrological Models in an R Package. *Environmental Modelling and Software*, 94, 166–171. DOI: 10.1016/j.envsoft.2017.05.002.
- Dewar, R.C., 2005: Maximum entropy production and the fluctuation theorem. *J. Phys. A* 38, L371–L381.
- Dewar, R.C., 2009: Maximum entropy production as an inference algorithm that translates physical assumptions into macroscopic predictions: don't shoot the messenger. *Entropy* 11, 931–944.
- Ficchi, A., 2017: *An adaptive hydrological model for multiple time-steps: Diagnostics and improvements based on fluxes consistency*. Doctoral dissertation, Irstea (Antony), GRNE (Paris), 281 pp. Accessible in [https://webgr.irstea.fr/wp-content/uploads/2017/09/2017-Thesis\\_final\\_Andrea\\_Ficchi\\_Irstea\\_2017.pdf](https://webgr.irstea.fr/wp-content/uploads/2017/09/2017-Thesis_final_Andrea_Ficchi_Irstea_2017.pdf)
- Fowler, A., 2002. Assessment of the validity of using mean potential evaporation in computations of the long-term soil water balance. *Journal of Hydrology* 256 (3-4), 248-263.

Givati, A., Gochis, D., Rummler, T. and Kunstmann, H. 2016: Comparing one-way and two-way coupled hydrometeorological forecasting systems for flood forecasting in the Mediterranean region. *Hydrology* 2016, 3, 19, doi:10.3390/hydrology3020019.

Gollan, T., Richards, R., Rawson, H., Passioura, J., Johnson, D. and Munns, R. 1986: Soil water status affects the stomatal conductance of fully turgid wheat and sunflower leaves. *Australian Journal of Plant Physiology* 13, 459-464.

Guo, D.L., Westra, S., Maier, H.R. 2017: Sensitivity of potential evapotranspiration to changes in climate variables for different Australian climatic zones. *Hydrol. Earth Syst. Sci.*, 2107-2126, <https://doi.org/10.5194/hess-21-2107-2017>.

Hajji, I., Nadeau, D., Music, B., Anctil, F., and Wang, J. 2017: Generalization and evaluation of the maximum entropy production method for estimating evapotranspiration.

Hamon, W.R., 1961. Estimating potential evapotranspiration. *Hydraul. Div. Proc. Am. Soc. Civil Eng.*, 87: 107-120.

Hobbins, M. T., J. A. Ramí' rez, and T. C. Brown (2004), Trends in pan evaporation and actual evapotranspiration across the conterminous U.S.: Paradoxical or complementary?, *Geophys. Res. Lett.*, 31, L13503, doi:10.1029/2004GL019846.

Hua, W. J., Chen, H. S., Zhu, S. G., et al. Hotspots of the sensitivity of the land surface hydrological cycle to climate change. *Chin Sci Bull*, 2013, 58: 3682-3688, doi: 10.1007/s11434-013-5846-7.

IPCC, 2014: *Climate Change 2014: Synthesis Report. Contribution of Working Groups I, II and III to the Fifth Assessment Report of the Intergovernmental Panel on Climate Change* [Core Writing Team, R.K. Pachauri and L.A. Meyer (eds.)]. IPCC, Geneva, Switzerland, 151pp.

Golubev, V. S., J. H. Lawrimore, P. Y. Groisman, N. A. Speranskaya, S. A. Zhuravin, M. J. Menne, T. C. Peterson, and R. W. Malone (2001), Evaporation changes over the contiguous United States and the former USSR: A reassessment, *Geophys. Res. Lett.*, 28, 2665–2668.

Gupta, H.V., Kling, H., Yilmaz, K.K., and Martinez, G.F., 2009: Decomposition of the mean squared error and NSE performance criteria: Implications for improving hydrological modeling. *Journal of Hydrology*, 377, 80-91.

Jaynes, E.T., 1957a: Information theory and statistical mechanics. *Phys Rev* 106 (4):620-630.

Jaynes, E.T., 1957b: Information theory and statistical mechanics, II. *Phys Rev* 106 (4): 171-190.

Jaynes, E.T. and Bretthorst, G.L. (Ed.) (2003): *Probability Theory – The logic of Science*, 755pp., Cambridge Univ. Press, New York.

Jasechko, S., Sharp, Z.D., Gibson, J.J., Birks, S.J., Y, Y., Fawcett, P.J.: 2013. Terrestrial water fluxes dominated by transpiration: *Nature*, 2013 Apr 18; 496(7445):347-50. doi: 10.1038/nature11983. Epub 2013 Apr 3.

Jung, M., et al. Recent decline in the global land evapotranspiration trend due to limited moisture supply. *Nature*, 467 (2010), pp. 951-954.

Kannan, N., et al., 2007. Sensitivity analysis and identification of the best evapotranspiration and runoff options for hydrological modelling in SWAT-2000. *Journal of Hydrology*, 332, 456-466, doi: 10.1016/j.jhydrol.2006.08.001.

Kay, A.L. and Davies, H.N., 2008. Calculating potential evaporation from climate model data: A source of uncertainty for hydrological climate change impacts. *Journal of Hydrology*, 358, 221-239, doi: 10.1016/j.jhydrol.2006.06.005.

Kingston, D. G., M. C. Todd, R. G. Taylor, J. R. Thompson, and N. W. Arnell (2009), Uncertainty in the estimation of potential evapotranspiration under climate change, *Geophys. Res. Lett.*, 36, L20403, doi:10.1029/2009GL040267.

Kleidon, A. *Naturwissenschaften* (2009) 96: Non-equilibrium thermodynamics and maximum entropy production in the Earth system. Doi:10.1007/s00114-009-0509-x

Kleidon, A., and Fraedrich, K. (2004): Biotic entropy production and global atmosphere-biosphere interaction, in non-equilibrium thermodynamics and the production of entropy, pp. 173-189, Springer, Heidelberg, Germany.

- Koster, R. D., et al. (2004), *Regions of strong coupling between soil moisture and precipitation*, *Science*, 305, 1138–1140, doi:10.1126/science.110021.
- Liu, B., M. Xu, M. Henderson, and W. Gong (2004), *A spatial analysis of pan evaporation trends in China, 1955–2000*, *J. Geophys. Res.*, 109, D15102, doi:10.1029/2004JD004511.
- Liu, Qiang & Yang, Zhifeng. (2010). *Quantitative estimation of the impact of climate change on actual evapotranspiration in the Yellow River Basin, China*. *Journal of Hydrology*. 395. 226-234. 10.1016/j.jhydrol.2010.10.031.
- Loumagne, C. and Tallec, G. (2013), *L'observation long terme en environnement, exemple du bassin versant de l'Orgeval*. Copyright at Edition Quae, Versailles Cedex, 335p. ISBN: 978-2-7592-2047-8.
- Loumagne, C., Chkir, N., Normand, M., Otlé, C., Vidal-Madjar, D. (1996): *Introduction of soil/vegetation/atmosphere continuum in a conceptual rainfall-runoff model*. *Hydrological Science Journal*, 41(6), 889-902.
- Maidment, D.R. (1993). *Handbook of hydrology*. New York, McGraw-Hill, p. 4.3.
- Martyushev, L.M. and Seleznev, V.D. *Maximum entropy production principle in physics, chemistry and biology*, *Physics Reports*, Volume 426, Issue 1, 2006, Pages 1-45, ISSN 0370-1573, doi: 10.1016/j.physrep.2005.12.001.
- Mercado, L. M., N. Bellouin, S. Sitch, O. Boucher, C. Huntingford, M. Wild, and P. M. Cox (2009), *Impact of changes in diffuse radiation on the global land carbon sink*, *Nature*, 458(7241), 1014–1017, doi:10.1038/nature07949.
- Monin, A. S. and Obukhov, A. M. (1954). *Basic laws of turbulent mixing in the surface layer of the atmosphere*. *Tr. Akad. Nauk. SSSR Geophys. Inst.* 24 (151): 163–187.
- Monteith, J.L. (1965): *Evaporation and environment*. *Symposia of the Society for Experimental Biology*. 19: 205-224.
- Morita, M. and Yen, B.C. (2000) *Numerical methods for conjunctive two-dimensional surface and three-dimensional sub-surface flows*. *Int J Numer Meth Fluids* 32:921–957.
- Myneni, R. B., Hall, F.G., Sellers, P.J., and Marshak, A.L. (1995): *The interpretation of spectral vegetation indexes*, *IEEE Transactions on Geoscience and Remote Sensing*, 33, 481-486.
- Nash, J.E. and Sutcliffe, J.V. 1970. *River flow forecasting through conceptual models part I-A discussion of principles*. *Journal of Hydrology*, 10, 282-290.
- Oudin, L. *Recherche d'un modèle d'évapotranspiration potentielle pertinent comme entrée d'un modèle pluie-débit global*. *Sciences of the Universe [physics]*. ENGREF (AgroParisTech), 2004. English. <pastel-00000931>
- Oudin, L., Andreassian, V., Perrin, C., and Anctil, F. (2004) *Locating the sources of low-pass behavior within rainfall-runoff models*, *Water Resour. Res.*, 40, W11101, doi: 10.1029/2004WR003291.
- Oudin, L., et al. (2005) *Should Bouchet's hypothesis be taken into account in rainfall-runoff modelling? An assessment over 308 catchments*. *Hydrol. Process*. 19, 4093-4106.
- Oudin, L., Michel, C., Anctil, F. *Which potential evapotranspiration input for a lumped rainfall-runoff model: Part 1 – Can rainfall-runoff models effectively handle detailed potential evapotranspiration inputs?* *J. Hydrol.*, 303 (1–4) (2005), pp. 275-289, 10.1016/j.jhydrol.2004.08.025.
- Oudin, L., et al. *Which potential evapotranspiration input for a lumped rainfall-runoff model: Part 2 –Towards a simple and efficient potential evapotranspiration model for rainfall-runoff modelling*. *J. Hydrol.*, 303 (1–4) (2005), pp. 275-289, 10.1016/j.jhydrol.2004.08.025.
- Parmele, L.H., 1972. *Errors in output of hydrologic models due to errors in input potential evapotranspiration*. *Water Resources Research* 3 (2), 348-359.
- Paturel, J.E., Servat, E., Vassiliadis, A., 1995. *Sensitivit* 3 (2), 348-359.
- Paturel, J.E., Servat, E., Vassiliadis, A., 1995. *Sensitivit of conceptual rainfall-runoff algorithms to errors in input data – case of the GR2M model*. *Journal of Hydrology* 168, 111-125.

- Perrin, C., Michel, C. and Andréassian, V. 2003. Improvement of a parsimonious model for streamflow simulation. *Journal of Hydrology* 279 (2003) 275-289.
- Pontailleur, J.Y., Hymus, G.J. and Drake, B.G. 2003: Estimation of leaf area index using ground-based remote sensed NDVI measurements: validation and comparison with two indirect techniques. *Canadian Journal of Remote Sensing*, 29, 381-387.
- Priestley, C.H.B., 1959: *Turbulent transfer in the lower atmosphere*, 130 pp., Univ. of Chicago Press, Chicago, III.
- Pushpalatha, R., Perrin, C., Moine, M.L., and Andréassian, V. 2012. A review of efficiency criteria suitable for evaluating low-flow simulations. *Journal of Hydrology* 420-421 (2012), 171-182.
- Qian, T., Dai, A., & Trenberth, K. E. (2007). Hydroclimatic trends in the mississippi river basin from 1948 to 2004. *Journal of Climate*, 20(18), 4599-4609,4611-4614.
- Roderick, M.L., & Farquhar, G.D. (2002). The cause of decreased pan evaporation over the past 50 years. *SCIENCE*. 298. 1410-1411.
- Roderick, M.L., & Farquhar, G.D. (2004). Changes in Australian pan evaporation from 1970-2002, *Int. J. Climatol.*, 24(9), 1077-1090, doi: 10.1002/joc.1061.
- Roderick, M.L., Hobbins, M.T., and Farquhar, G.D.(2009a). Pan evaporation trends and the terrestrial water balance: II. Energy balance and interpretation, *Geogr. Compass*, 3(2), 761-780, doi:10.1111/j.1749-8498.2008.0024.x.
- Seguin B. (1997) Areal Evaporation from Satellite Thermal Infrared Data. In: Sorooshian S., Gupta H.V., Rodda J.C. (eds) *Land Surface Processes in Hydrology. NQTO ASI Series (Series I: Global Environmental Change)*, vol 46. Springer, Berlin, Heidelberg, p:281.
- Seiller, G., and Anctil, F. (2016) How do potential evapotranspiration formulas influence hydrological projections?, *Hydrological Science Journal*, 61: 12, 2249-2266, doi: 10.1080/02626667.2015.1100302.
- Shannon, C.E., 1948a: A mathematical theory of communication. *Bell Syst Tech J* 27(3): 379- 423.
- Shannon, C.E., 1948b: A mathematical theory of communication. *Bell Syst Tech J*27(4): 623-659.
- Sharma AN, Walter MT (2014) Estimating long-term changes in actual evapotranspiration and water storage using a one-parameter model. *J Hydrol* 519:2312–2317.
- Singh, V.P.& Xu, C.Y. (1997) Evaluation and generalization of 13 equations for determining free water evaporation. *Hydrological Process*, 11(3): 311-323.
- Stewart, J.B., and Thom, A.S. (1973), Energy budgets in pine forest, *Quart. J. Roy. Meteorol. Soc.* 99, 154-170.
- Swenson, R. (2000). *Spontaneous Order, Autocatakinetic Closure, and the Development of Space-Time*. *Annals New York Academy of Sciences*, vol. 901, pp. 311-319, 2000.
- Tetens, O., 1930. *Uber einige meteorologische Begriffe*. z. *Geophys.* 6:297-309.
- Teuling, A.J., et al. (2009), A regional perspective on trends in continental evaporation, *Geophys. Res. Lett.*, 36, L02404, doi: 10.1029/2008GL036584.
- Thornthwaite, C.W. (1948) *An approach toward a rational classification of climate*, *Geograph. Rev.* 38, 55-94.
- Turc, L., 1961. Estimation of irrigation water requirement, potential evapotranspiration: a simple climatic formula evolved up to date. *Annals of Agronomy*, 12 (1): 13-49.
- Van Heerwaarden, C. C., J. Vilà -Guerau de Arellano, and A. J. Teuling (2010), Land-atmosphere coupling explains the link between pan evaporation and actual evapotranspiration trends in a changing climate, *Geophys. Res. Lett.*, 37, L21401, doi:10.1029/2010GL045374.
- Vidal, J.P., Martin, E., Franchistéguy, L., Baillon, M., and Soubeyroux, J.M.(2010). A 50-year high-resolution atmospheric reanalysis over France with the Safran system, *Int. J. Climatol.* 30 (2010) 1627-1644.
- Wang, J., and Bras, R.L. (2009), A model of surface heat fluxes based on the theory of maximum entropy production, *water Resour. Res.*, 45, W11422, doi: 10.1029/2009WR007900.

- Wang, J., and Bras, R.L. (2011), A model of evapotranspiration based on the theory of maximum entropy production, *Water Resour. Res.*, 47, W03521, doi: 10.1029/2010WR009392.
- Wang, K., & Dickson, R.E. (2012) A review of global terrestrial evapotranspiration: Observation, modeling, climatology, and climatic variability, *Rev. Geophys.*, 50, RG2005, doi: 10.1029/2011RG000373.
- Wang, Y.P., and Leuning, R. 1998: A two-leaf model for canopy conductance, photosynthesis and partitioning of available energy I: Model description and comparison with a multi-layered model. *Agricultural and Forest Meteorology*, 91, 89-111.
- Wu, W.R., and Dickinson, R.E. 2004. Time scales of layered soil moisture memory in the context of land-atmosphere interaction: *Journal of Climate*, 17: 2752-2764.
- Xu, C.Y., et al. (2005) Analysis of spatial distribution and temporal trend of reference evapotranspiration and pan evaporation in Changjiang (Yangtze River) catchment, *Journal of Hydrology*, 327: 81-93, doi: 10.1016/j.jhydrol.2005.11.029.
- Zabel, F. and Mauser, W. 2012. 2-way coupling the hydrological land surface model PROMET with the regional climate model MM5. *Hydrol. Earth Syst. Sci.*, 17, 1705-1714, 2013. Doi: 10.5194/hess-17-1705-2013.
- Zhao, L.L, J. Xia, C.Y. Xu, Z.G. Wang, L. Sobkowiak, C. Long. Evapotranspiration estimation methods in hydrological models. *J. Geog. Sci.*, 23 (2) (2013), pp. 359-369
- Zhang, L., Dawes, W.R., and Walker, G.R. (2001) Response of mean annual evapotranspiration to vegetation changes at catmint scale. *Water Resources Research*, Vol. 37, No.3, p 701-708.
- Zhang, Y.Q., Chiew, F.H.S., Zhang, L., and Li, H.X. 2009. Use of remotely sensed actual evapotranspiration to improve rainfall-runoff modeling in Southeast Australia. *J. Hydrometeorol* (2009). Doi: 10.1175/2009JHM1061.1;
- Zotarelli, L., Dukes, M. and Morgan, K. 2010: Interpretation of soil moisture content to determine soil field capacity and avoid over-irrigating sandy soils using soil moisture sensors. *The agricultural and Biological Engineering Department, Florida Cooperative Extension Service, Institute of Food and Agricultural Sciences, University of Florida, AE460.*

## Appendix

### 1. The MEP model formulation

The MEP principle comes down to the dissipation function or the entropy production function:

$$D \equiv 2 \sum_{k=1}^m \lambda_k F_k \quad (1)$$

where  $\lambda_k$  ( $1 \leq k \leq m$ ) are the Lagrange multipliers associated with the given constraints  $F_k$  ( $1 \leq k \leq m$ ) and  $\lambda_k$  must be expressed as explicit functions of  $F_k$  (Dewar, 2005). By seeking the extreme of the dissipation function, the most likely evolution can thus be speculated. Analogously, dissipation functions for resolving ET restricted under the energy conservation can be outlined in two situations: bare-soil and vegetated land surface.

#### 1) Bare-soil land surface

The dissipation function is formulated as:

$$D(E, H, G) \equiv \frac{2G^2}{I_s} + \frac{2H^2}{I_a} + \frac{2E^2}{I_e} \quad (2)$$

where  $G$ ,  $H$  as well as  $E$  are the ground, sensible and latent heat flux ( $Wm^{-2}$ ) respectively. The corresponding  $I_s$ ,  $I_a$  and  $I_e$  are the thermal inertia parameters ( $Wm^{-2}K^{-1}s^{1/2}$ ) to each heat flux.

The physically-based parameter  $I_s$ , defined as the saturated soil thermal inertia here can be calculated as:

$$I_s = I_{ds} + \sqrt{\theta} I_w \quad (3)$$

where  $\theta$  is the volumetric soil moisture;  $I_{ds} = \sqrt{\rho_{ds} c_{ds} k_{ds}}$  the thermal inertia of local dry soil with  $\rho_{ds}$  the density (vary between  $1.0 \sim 1.6 \times 10^3 \text{ kgm}^{-3}$ ),  $c_{ds}$  the specific heat (around  $0.8 \text{ kJkg}^{-1}K^{-1}$ ) and  $k_{ds}$  the heat conductivity (in most cases less than  $0.5 \text{ Wm}^{-1}K^{-1}$ );  $I_w = \sqrt{\rho_w c_w k_w}$  the thermal inertia of liquid water with  $\rho_w$  the density ( $1.0 \times 10^3 \text{ kgm}^{-3}$ ),  $c_w$  the specific heat ( $4.18 \text{ kJkg}^{-1}K^{-1}$ ) and  $k_w$  the heat conductivity ( $0.58 \text{ Wm}^{-1}K^{-1}$ ). Alternatively, a global map of  $I_s$  analytical solution was produced by Bennett *et al.* (2008) in six-hour, daily and monthly temporal resolution, which is applied in the work of Peredo (2017).

$I_a$ , the quasi thermal inertia for turbulent heat conduction in the air, is deduced from the eddy diffusivity and temperature gradient based on Monin-Obukhov similarity theory (MOST) (Monin and Obukhov, 1954; Arya, 1988; Wang and Bras, 2009). It is expressed as:

$$I_a = \rho C_p \sqrt{C_1 \kappa z} \left( C_2 \frac{\kappa z g}{\rho C_p T_0} \right)^{\frac{1}{6}} |H|^{\frac{1}{6}} \equiv I_0 |H|^{\frac{1}{6}} \quad (4)$$

where  $I_0$  is referred to as the ‘‘apparent thermal inertial of the air’’, which depends only on external parameters,  $z$  the vertical coordinate ( $m$ ) and  $T_0$  the reference

temperature ( $\sim 300\text{ K}$ ). The internal parameters  $\rho$ ,  $C_p$ ,  $\kappa$  and  $g$  are the air density ( $1.22\text{ kgm}^{-3}$ ), the heat capacity of air ( $1.00\text{ kJkg}^{-1}\text{K}^{-1}$ ), the Von Karman constant (0.40) and the gravitational acceleration ( $9.81\text{ ms}^{-2}$ ) respectively. The empirical coefficients  $C_1$  and  $C_2$  of the extremum solution of MOST are taken as follows:

$$C_1 = \begin{cases} \sqrt{3}/\alpha, & \text{unstable} \\ 2/(1+2\alpha), & \text{stable} \end{cases}$$

$$C_2 = \begin{cases} \gamma_2/2, & \text{unstable} \\ 2\beta, & \text{stable} \end{cases}$$

where the constants are estimated as  $\alpha \sim 0.75$  or  $1$ ,  $\beta \sim 4.7$ ,  $\gamma_2 \sim 9$ . The stable empirical coefficients are applied for nocturnal periods, while the unstable ones are for the diurnal periods. A detailed derivation procedure of  $I_a$  can be found in the *Appendix B* given in Wang and Bras (2009).

The parameter  $I_e$ , the quasi thermal inertia for the transport of latent heat accompanied by the movement of water vapor in the atmospheric boundary layer (ABL) and the flow of liquid water in the soil (Wang and Bras, 2011), is proposed as an exploratory analogy of  $I_a$ .

$$I_e \equiv \sigma I_a \quad (5)$$

A dimensionless coefficient  $\sigma$  is introduced as the transition layer from soil to air which characterizes the state of the evaporating surface:

$$\sigma = \frac{\lambda^2 q_s}{C_p R_v T_s^2} \quad (6)$$

where external parameters are  $T_s$  the skin soil temperature ( $K$ ) and  $q_s$  the surface specific humidity ( $kg/kg$ ).  $\lambda$ ,  $R_v$  and  $C_p$  are the latent heat of vaporization liquid water ( $\sim 2501 - 2.36(T_s - 273.15)$ ,  $kJ/kg$ ), the gas constant for water vapor ( $461.5\text{ Jkg}^{-1}\text{K}^{-1}$ ) and the heat capacity of air ( $1.00\text{ kJkg}^{-1}\text{K}^{-1}$ ), respectively. The arguments of the experience-based or inferred postulation on  $\sigma$  are expanded in the *Appendix A* in Wang and Bras (2011). When in lack of  $q_s$  observation data,  $q_s$  can be willingly estimated from the Clausius-Clapeyron equation where relative humidity and temperature are needed (see *Appendix A1*).

Hence, under the energy conservation for a supposed net radiation  $R_n$ :

$$R_n = G + H + E \quad (7)$$

and by minimizing the dissipation function  $D(E, H, G)$  as the constraint condition is a linear function (Dewar, 2005), surface heat flux can be deduced.

$$G = \frac{B(\sigma) I_s}{\sigma I_0} H |H|^{-\frac{1}{6}} \quad (8)$$

$$E = B(\sigma) H \quad (9)$$

$B(\sigma)$  here is formulated as the function below,

$$B(\sigma) = 6 \left( \sqrt{1 + \frac{11}{36} \sigma} - 1 \right) \quad (10)$$

which refers to the reciprocal relationship of Bowen ratio (Bowen, 1926) and it

strongly accords with the classical Priestley model whose application in land surface is inconvenient due to the parameterization process (Priestley, 1959; Wang and Bras, 2011). Finally, the bare soil evaporation  $E_v$  can be obtained in  $mm/s$ .

$$E_v = \frac{E}{\rho_w \lambda} \quad (11)$$

## 2) Vegetated land surface

Following the pattern above, the MEP principle can be applied to a vegetated land surface. As a limiting case of bare-soil, when  $I_s \approx 0$  due to the negligible leaf surface thermal inertia number, whose magnitude is smaller than two to three orders compared with that of the soil, only transpiration is considered (Wang and Bras, 2011). Thus, the leaf surface heat flux  $G$  can be neglected and the entered energy, net solar radiation, is carved up by sensible as well as latent heat flux on the leaf surface.

The term  $E$ , latent heat flux, and  $H$ , the sensible heat flux, can be expressed as:

$$E = \frac{Rn}{1 + B^{-1}(\sigma)} \quad (12)$$

$$H = \frac{Rn}{1 + B(\sigma)} \quad (13)$$

where  $B(\sigma)$  is given in equation (10) and  $\sigma$  in equation (6). Note that  $T_s$  ( $K$ ) and  $q_s$  ( $kg/kg$ ) represent the leaf temperature and leaf surface specific humidity. The vegetal transpiration  $T_r$  can thus be calculated in  $mm/s$ .

$$T_r = \frac{E}{\rho_w \lambda} \quad (14)$$

Here  $T_s$  is considered as a homogeneous temperature of air. Since  $q_s$  is rarely measured, it is usually taken as the air specific humidity. However, leaf surface specific humidity does not always agree with that of the air because of the stomatal openness. The difference can be large in period of water stress when restricted water availability from soil may result in stomatal closure and reduce the rates of transpiration. A relation between leaf surface specific humidity  $q_s$  and air specific humidity  $q_a$  is proposed by the work of Hajji *et al.* (2017), with the introduction of stomatal aperture parameter  $\eta_s$ , which is formulated as:

$$q_s = \eta_s q_a \quad (15)$$

where  $0 \leq \eta_s \leq 1$  represents the full range of water supply conditions.

Water availability for plants can be empirically related to the soil moisture  $\theta$  in the root zone and the formulation of stomatal conductance  $\eta_s$  is given by Wang and Leuning (1998, equation (7)) which is similar to that of Gollan *et al.* (1986). The empirical function is expressed as:

$$\eta_s(\theta) = \min\left(1, \frac{10(\theta - \theta_{\min})}{3(\theta_{\max} - \theta_{\min})}\right) \quad (16)$$

where  $\theta_{\max}$  and  $\theta_{\min}$  are soil water content in root zone at field capacity and wilting point respectively, which can be estimated from soil characteristics. In addition to this, by taking the 99<sup>th</sup> and 1<sup>st</sup> percentile of the long-term soil moisture observations,  $\theta_{\max}$  and  $\theta_{\min}$  can also be acquired when soil type is unknown (Zotarelli *et al.*, 2010;

Hajji, 2017).

### 3) Vegetation Index

Chlorophyll in plant leaves preferentially absorbs solar radiation in the photosynthetically active spectrum, which is in the red portion, and strongly reflects the near-infrared to avert overheating (Myneni, 1995). Therefore, the evolution of green vegetation cover at the catchment scale can be measured by analyzing the reflection spectrum of solar radiation. As a product of satellite remote sensing, the Normalized Difference Vegetation Index (NDVI) indicates the chlorophyll activity and is defined as follow:

$$NDVI = \frac{IR - R}{IR + R} \quad (17)$$

where  $IR$  and  $R$  stand for the spectral reflectance measurements acquired in near-infrared and red regions, respectively. The NDVI-based research has been widely investigated in earth science (e.g., Pontailier, 2003; Bhatt *et al.*, 2010). Wittich and Hansing (1995) gave the vegetative cover fraction based on NDVI data:

$$f_{veg} = \frac{NDVI - NDVI_{min}}{NDVI_{max} - NDVI_{min}} \quad (18)$$

where  $NDVI_{max}$  and  $NDVI_{min}$  represent the exuberant vegetation (approximately 0.8) and the bare soil (around 0.1 or less).

The ET process is the combination of the evaporation from bare soil and the transpiration from vegetation. With the introduction of vegetation index  $f_{veg}$  which indicates the scale of vegetation for a certain land surface, we can finally obtain the ET formula as:

$$ET = (1 - f_{veg})E_v + f_{veg}T_r \quad (19)$$

where  $E_v$  and  $T_r$  are given in equation (11) and (14).

### 2. Estimation of specific humidity from the Clausius-Clapeyron equation

Firstly, we start from specific humidity  $q$  ( $kgkg^{-1}$ ) and it is defined as the mass of water vapor in a unit mass of moist air.

$$q \equiv \frac{m_{water}}{m_{water} + m_{air}} = \frac{w}{w + 1} \approx w$$

where  $m_{water}$  is the mass of water vapor ( $kg$ ),  $m_{air}$  the mass of moist air ( $kg$ ),  $w$  the mass ratio of water vapor and moist air.

Relative humidity  $RH$  (%) is the present amount of water in the air compared to the greatest amount it would be possible for the air to hold at the present temperature. Thus, it can be expressed as the ratio of the present specific humidity and the saturated specific humidity.

$$\left\{ \begin{array}{l} RH = \frac{q}{q_{saturate}} \times 100 \approx \frac{w}{w_{saturate}} \times 100 \\ w_{saturate} \equiv \frac{m_{water\ saturate}}{m_{air}} = \frac{e_s/R_v}{(p - e_s)/R_d} \approx 0.622 \frac{e_s}{p} \end{array} \right.$$

where  $e_s$  is the saturation vapor pressure ( $Pa$ ),  $p$  the moist air pressure ( $Pa$ ),  $R_v$  the specific gas constant for water vapor ( $Jkg^{-1}K^{-1}$ ),  $R_d$  the specific gas constant for dry air ( $Jkg^{-1}K^{-1}$ ).

From the Clausius-Clapeyron equation, saturation vapor pressure can be estimated as follow:

$$e_s(T) = e_{s0} e^{\frac{\lambda}{R_v} \left( \frac{1}{T_0} - \frac{1}{T} \right)} \approx 611 e^{\frac{17.67(T-T_0)}{T-29.65}}$$

where  $\lambda$  is the latent heat of vaporization liquid water ( $Jkg^{-1}$ ),  $T_0$  the reference temperature (typically 273.16 K) and  $T$  the temperature (K).

Once the relative humidity  $RH$  and the temperature  $T$  is known, the specific humidity  $q$  can therefore be obtained.

$$q \approx w = \frac{RH}{100} w_{saturate} \approx \frac{RH e^{\frac{17.67(T-T_0)}{T-29.65}}}{0.263P}$$

### 3. Penman-Monteith potential evapotranspiration

The potential evapotranspiration produced from Penman-Monteith formula (Monteith, 1965) approximates the atmospheric demand for water from a saturated surface, mainly considering these meteorological parameters as temperature, wind speed, specific humidity and solar radiation.

$$\begin{cases} ET = \frac{\Delta R_n + \rho_a C_p \delta \frac{1}{r_a}}{(\Delta + \gamma \left( 1 + \frac{r_s}{r_a} \right)) L_v} \\ \Delta = \frac{4098 (0.618 e^{\frac{17.27T}{T+237.3}})}{(T + 237.3)^2} \end{cases}$$

where  $ET$  is the water volume from evapotranspiration ( $mm s^{-1}$ ),  $T$  the temperature ( $^{\circ}C$ ),  $L_v$  the volumetric latent heat of vaporization ( $\sim 2543 MJ m^{-3}$ ),  $\Delta$  the rate of change of saturation specific humidity with air temperature ( $Pa^{\circ}C^{-1}$ ),  $R_n$  the net radiation ( $W m^{-2}$ ),  $C_p$  the specific heat capacity of air ( $Jkg^{-1}^{\circ}C^{-1}$ ),  $\rho_a$  dry air density ( $kg m^{-3}$ ),  $\delta$  the vapor pressure deficit ( $Pa$ ) which is the difference between the saturated vapor pressure and the actual vapor pressure,  $r_a$  the aerodynamic resistance ( $sm^{-1}$ ),  $r_s$  the resistance to flux from a vegetation canopy ( $sm^{-1}$ ) and  $\gamma$  the psychrometric constant ( $\sim 66 Pa^{\circ}C^{-1}$ ).

The saturated vapor pressure  $e_s$  ( $Pa$ ) can be estimated from Tetens formula (1930) as follow.

$$e_s = 0.618 e^{\frac{17.27T}{T+237.3}}$$

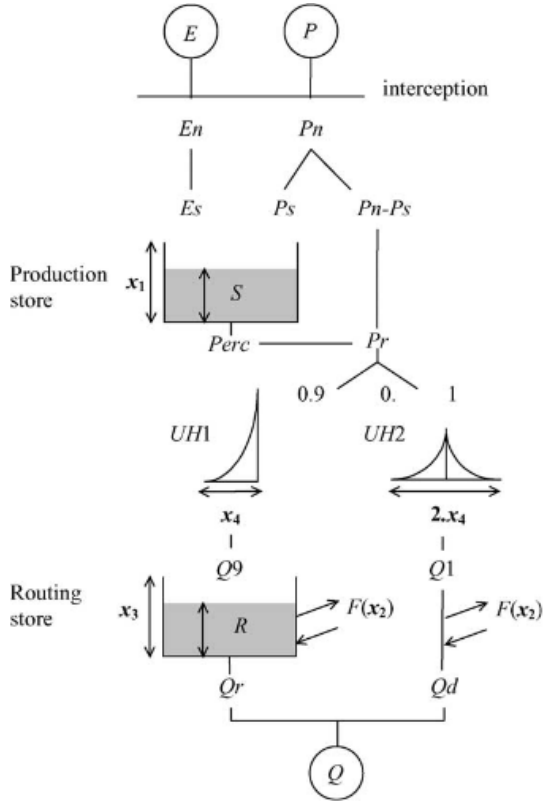
And the actual vapor pressure  $e_a$  ( $Pa$ ) can be derived from  $q_s$  ( $kg kg^{-1}$ ) the current specific humidity and  $P_{atm}$  ( $kPa$ ) the atmospheric pressure.

$$\begin{cases} P_{atm} = 101.325 \left( \frac{288 - 0.0065z}{288} \right)^{5.255} \\ e_a = \frac{P_{atm} q_s}{\varepsilon + (1 - \varepsilon) q_s} \end{cases}$$

where  $\varepsilon$  is the ratio of the molecular weights between air and water ( $\sim 0.622$ ).

The aerodynamic resistance  $r_a$  here is calculated as the reciprocal of wind speed at the 2 m height while the local surface resistance  $r_s$  is parameterized to 70 ( $sm^{-1}$ ).

#### 4. Interception process and the production store evolution in GR4H model



Interception: determination of net PET and net P

*if  $P \geq E, P_n = P - E$  and  $E_n = 0$*

*Otherwise,  $P_n = 0$  and  $E_n = E - P$*

Production Store: soil moisture accounting

*if  $P_n > 0$ , rain fills the production store*

$$P_s = \frac{x_1 \left( 1 - \left( \frac{S}{x_1} \right)^2 \right) \tanh \left( \frac{P_n}{x_1} \right)}{1 + \frac{S}{x_1} \tanh \left( \frac{P_n}{x_1} \right)}$$

*if  $E_n > 0$ , AET extracts the production store*

$$E_s = \frac{S \left( 2 - \frac{S}{x_1} \right) \tanh \left( \frac{E_n}{x_1} \right)}{1 + \left( 1 - \frac{S}{x_1} \right) \tanh \left( \frac{E_n}{x_1} \right)}$$

Water content changes:

$$S = S - E_s + P_s$$

Percolation leakage:

$$Perc = S \left\{ 1 - \left[ 1 + \left( \frac{4S}{9x_1} \right) \right]^{-1/4} \right\}$$

Water content updates:

$$S = S - Perc$$

**Figure 5a:** The diagram of GR4H model (Source: Perrin *et al.*, 2003 in page 3).